Received: 12 September 2023 | Revised: 13 December 2023 | Accepted: 15 December 2023

DOI: 10.1002/jcc.27299

RESEARCH ARTICLE

Journal of COMPUTATIONAL CHEMISTRY WILEY

Development of a multi-step screening procedure for redox active molecules in organic radical polymer anodes and as redox flow anolytes

Andreas J. Achazi[1,2] | Xhesilda Fataj[3,4] | Philip Rohland[3,4] | Martin D. Hager[3,4] | Ulrich S. Schubert[3,4] | Doreen Mollenhauer[1,2]

[1]Physikalisch-Chemisches Institut, Justus-Liebig-Universität Gießen, Gießen, Germany

[2]Zentrum für Materialforschung, Justus-Liebig-Universität Gießen, Gießen, Germany

[3]Laboratory of Organic and Macromolecular Chemistry (IOMC), Friedrich Schiller University Jena, Jena, Germany

[4]Center for Energy and Environmental Chemistry Jena (CEEC Jena), Friedrich Schiller University Jena, Jena, Germany

Correspondence
Andreas J. Achazi and Doreen Mollenhauer, Physikalisch-Chemisches Institut, Justus-Liebig-Universität Gießen, Heinrich-Buff-Ring 17, 35392 Gießen, Germany.
Email: andreas.achazi@phys.chemie.uni-giessen.de and doreen.mollenhauer@phys.chemie.uni-giessen.de

Funding information
Deutsche Forschungsgemeinschaft

Abstract

Benzo[*d*]-X-zolyl-pyridinyl (X═O, S, NH) radicals represent a promising class of redox-active molecules for organic batteries. We present a multistep screening procedure to identify the most promising radical candidates. Experimental investigations and highly correlated wave function-based calculations are performed to determine benchmark redox potentials. Based on these, the accuracies of different methods (semi-empirical, density functional theory, wave function-based), solvent models, dispersion corrections, and basis sets are evaluated. The developed screening procedure consists of three steps: First, a conformer search is performed with CREST. The molecules are selected based on the redox potentials calculated using GFN2-xTB. Second, HOMO energies calculated with reparametrized B3LYP-D3(BJ) and the def2-SVP basis set are used as selection criteria. The final molecules are selected based on the redox potentials calculated from Gibbs energies using BP86-D3(BJ)/def2-TZVP. With this multistep screening approach, promising molecules can be suggested for synthesis, and structure–property relationships can be derived.

KEYWORDS
DFT, multi-step screening, organic redox flow battery, polymer-based batteries, viologen

1 | INTRODUCTION

In recent years, research on redox flow batteries (RFBs) has shifted from metal-based to organic active materials.[1,2] Organic materials are less expensive than metal-based materials,[1,3] cause less environmental damage,[1,3] and may be synthesized from renewable resources in the future.[4] The organic, redox active molecules for RFBs can also be used in organic polymer-based batteries (PBBs). For example, the most prominent material, the commonly used 2,2,6,6-tetramethylpiperidin-1-oxyl (TEMPO), has been employed as a redox-active cathode material in both organic RFBs and PBBs (see ESI for more details on RFBs and PBBs).[1,4] In aqueous solution, TEMPO has an oxidation potential of 0.722 V versus the normal hydrogen electrode (NHE).[5] A compatible redox-active anode material must have a significantly lower potential for its redox reaction. Many different organic molecules are currently being investigated for use as anode material.[1,4,6,7] Viologens have demonstrated desirable redox potentials and stability for use in organic RFBs and PBBs.[8–13] However, it is difficult to chemically modify viologens to optimize their properties, such as their redox potential. To improve viologens, one of the pyridyl groups is

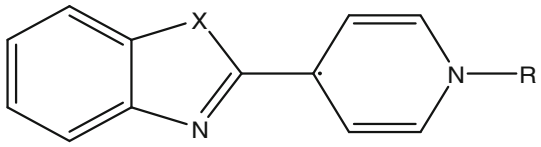

1-X-R

SCHEME 1 Schematic representation of the general structure **1-X-R** for the molecules studied. 4-(Benzo[*d*]-X-zol-2-yl)-1-methyl-1,4-dihydropyridin-4-yl radicals where X═O, S, NH and R═Me, Bn.

replaced by a benzo[*d*]-X-zolyl group. This leads to the general structure **1-X-R** shown in Scheme 1. Three different heteroatomic groups can be introduced at the X-position: O, S, and NH. Different organic groups R can also be introduced. R is the linker to the polymer chain in PBBs and can be freely chosen for RFBs. In addition, the four hydrogens at the benzo group can be replaced by functional groups such as —CH_3, —CF_3, —CN, —OH, and —OCH_3. This results in a large number of differently substituted **1-X-R**-type molecules.

A first experimental study by Savarino et al.[14] on the redox properties of **1-X-R**-type molecules with an unsubstituted benzo group is promising. However, the substituents and substitution pattern are important for optimizing the properties. In addition to other studies[15,16] we have carried out in the field, our study[17] on the redox potentials of a large number of substituted quinones revealed, for example, the non-intuitive effects of substituents and substituent patterns on the redox potentials in addition to the expected influences on them. The lowest redox potentials were not found for the fully substituted quinones. Inductive effects had only a little influence on the redox potential. Instead, the substituents with large negative resonance effects (—CN, —NO_2) revealed the strongest impact. We also found that intramolecular hydrogen bonds allow higher values of the redox potentials. Thus, the best candidates are not necessarily obvious.

To find the best candidate and novel redox-active molecules for an organic RFB or PBB, computational screening methods can be used.[17–25] For example, Li et al.[22] screened 660 molecules for a candidate with a low reduction potential molecule for a PBB. The authors used a semi-empirical extended tight binding method together with a trained Gaussian process regression model to select the 10% with the lowest reduction potential. These top 10% predicted molecules were then further calculated with density-functional theory (DFT) to identify the most promising redox-active molecules. Two other extensive high-throughput screenings were performed by Cheng et al.[20] and Duke et al.[25] In the former, about 1400 organic molecules were screened in 2015, and in the latter, 43,000 organic molecules were screened in 2023 for RFBs in a multistep approach based on DFT. Redox potentials can be predicted faster and with higher accuracy compared to other properties such as solubility and stability.[17,18] Knowing the redox potentials makes it possible to estimate the maximum voltage of the battery. The redox potentials are calculated from the Gibbs energies of the redox reactions.[26] However, Bachmann et al. showed that the energy of lowest unoccupied orbital (LUMO) can also be used instead of Gibbs energy.[23]

In the present study, a computational screening procedure is developed to determine the oxidation and reduction potentials of **1-X-R**-type molecules, which are radicals (Scheme 1). In organic synthesis, cationic species are generated in the first step.[27] Therefore, experimental studies are preferably presented from the perspective of the cationic species. For a better understanding, however, the theoretical study is presented from the perspective of the radical. The aim of the screening approach is to identify **1-X-R**-type radicals (Scheme 1) that have either a very low oxidation potential or a high reduction potential. A low oxidation potential enables a higher cell voltage and, therefore, a higher specific energy density. A higher reduction potential would make the reduction reaction assessable for use in the battery. Oxidation and reduction can then take place at the anode to store two electrons per redox-active molecule. This would also increase the specific energy density of the battery. As in previous studies,[17–25] both Gibbs energies and orbital energies approaches are investigated for the calculation of the redox potentials. Different methods [semi-empirical, DFT (27 density functionals), and wave function-based], dispersion corrections (three different ones), and basis sets are utilized to calculate the oxidation and reduction potentials of **1-X-R**-type molecules. Fornari et al.[18] identified the implicit solvent models as the main source of error for DFT-based calculations of redox potentials. Therefore, nine different implicit solvent models and settings are investigated in the presented study. Q. Zhang et al.[24] and W. Zhang et al.[28] carried out a method validation of density functionals (DFs) for determining the redox potentials of redox-active molecules. Q. Zhang et al. focused on quinones and made a comparison with experimental data.[24] W. Zhang et al.[28] employed the redox potentials of 10 solvents regularly used in electrolytes for lithium metal batteries. The benchmark values were generated by W. Zhang et al. themselves using higher level wave function-based methods.[28]

In contrast, this study includes benchmark values from both experiments and higher-level wave function-based methods in parallel. This provides additional information on the deviations between calculations and experiments, and allows for the identification of possible sources of error. Furthermore, additive terms for DFT and different parameterizations of DFs for the calculation of the redox potentials of type **1-X-R** molecules are developed in the present study. Finally, a multistep procedure for the screening of type **1-X-R** molecules is presented. It consists of three steps. First, a conformer search and screening are performed with a semi-empirical extended tight binding method. Second, redox potentials are estimated from orbital energies at the DFT level. Finally, DFT is used to calculate the Gibbs energies and the redox potentials.

2 | COMPUTATIONAL DETAILS

2.1 | Molecules of interest and experimental reference data

The basic structures of the **1-X-R**-type molecules selected in the present study are shown in Scheme 2. The experimental oxidation and

reduction potential are also given in Scheme 2. The redox potentials were measured in acetonitrile using a standard three-electrode setup. $Ag/AgNO_3$ (0.01 M) was used as the reference electrode. A glassy carbon (GC) electrode served as a working electrode, and a platinum (Pt) wire served as counter electrode. The electrolyte used was tetrabutylammonium hexafluorophosphate. More details of the experimental details are in reference.[27]

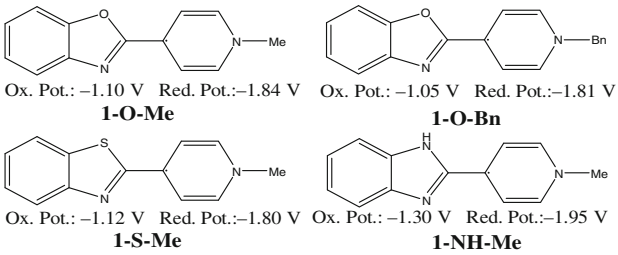

SCHEME 2 **1-X-R**-type molecules (see Scheme 1) where X═O, S, NH; and R═Me, Bn. The experimental oxidation potential and reduction potentials were measured in acetonitrile against an $Ag/AgNO_3$ (0.01 M) reference electrode.

2.2 | Computational methods

2.2.1 | Conformer search using extended tight-binding approach

A conformer search for the oxidized (cation), radical (neutral), and reduced (anion) species of the molecules of interest (Scheme 2) was performed using the CREST program package.[29–31] The aim was to find the starting structures for the DFT calculations and the calculations of the redox potentials. The conformer search was performed in two steps. First, the iterative meta-dynamics with a genetic structure crossing (iMTD-GC) algorithm was utilized. Then, structure optimization was performed using the extended tight-binding model GFN2-xTB.[32–34] The solvent acetonitrile was simulated in these calculations using the implicit analytical linearized Poisson-Boltzmann (ALPB) and generalized Born with surface area (GBSA) solvent models.[35] Conformers up to 125 kJ mol^{-1} above the lowest energy structure at the GFN2-xTB (ALPB) and GFN2-xTB (GBSA) levels of theory were considered.

2.2.2 | DFT calculations

All calculations were performed using the Turbomole 7.5.1 software package.[36–38] In some cases, the Gaussian 16 C.01 program package was used,[39] which is then specifically mentioned.

Conformer search and structural optimization at the DFT level

The conformers found at the GFN2-xTB (ALPB) and (GBSA) levels of theory, all lowest energy conformers, and other promising conformers up to 125 kJ mol^{-1} above the lowest energy structure were selected. Additional promising conformer structures that were not found in the conformer search were manually generated. This was done for the oxidized, radical, and reduced species of all molecules of interest (Scheme 2). From all these conformers, the lowest energy structures were determined using DFT.

The density functional (DF) used for the structural optimization was B3LYP[40–45] in conjunction with the dispersion correction DFT-D3[46] with Becke-Johnson-damping[47] [abbreviated here as B3LYP-D3(BJ)]. The polarized triple-ζ basis set def2-TZVP was employed unless otherwise stated.[48,49] B3LYP is generally considered to be a reliable DF,[50,51] in particular when combined with the D3(BJ) dispersion correction and the def2-TZVP basis set.[51] Furthermore, the Resolution-of-Identity (RI) approximation,[49,52,53] and the "multiple grid" m4 were utilized (see ESI).[54] The dielectric continuum solvent model COSMO (conductor-like screening model)[55,56] was used to simulate the solvent acetonitrile (relative permittivity $\varepsilon_r = 37.5$,[57] refractive index $n_D = 1.3442$[58]), which was used in the experiments.[27] The convergence criteria for the structure optimization were set to 10^{-8} E_h and 10^{-4} E_h a_0^{-1} for the energy and gradient, respectively. The structures were verified as energetic minima by calculating the vibrational frequencies. The calculations were carried out with the Turbomole script NumForce, including the fast contribution of the solvent.[59,60] At this B3LYP-D3(BJ)/def2-TZVP (COSMO) level of theory, the lowest energy structures were selected. These served as starting structures for all other DFT and wave function-based calculations.

Variation of the dispersion correction, basis set, solvent model and DF

The preoptimized equilibrium structures were reoptimized and their energies recalculated with different DFs, dispersion corrections, basis sets, and solvent models. For the convergence criteria, the energy and gradient were converged to 10^{-6} E_h and 10^{-3} E_h a_0^{-1}, respectively. For BP86-D3(BJ) (COSMO), the energy and gradient convergence were set to 10^{-8} E_h and 10^{-4} E_h a_0^{-1}. As before, the RI-approximation and the grid m4 were used for the calculations.

The dispersion corrections D4[61,62] and VV10[63,64] were utilized in conjunction with the B3LYP DF, the def2-TZVP basis set, and the COSMO solvation model. In addition, B3LYP-D3(BJ) (COSMO) calculations were performed with the def2-XVP (X = S, QZ),[49,54,65] def2-SVPD,[49,66] and def2-XVPPD (X = TZ, QZ)[49,66] basis sets. Finally, B3LYP-D3(BJ)/def2-TZVP was employed with a total of nine different solvation models or settings for the solvation model. Four different variants and settings for the COSMO solvation model were tested. They are here referred to as "COSMO", "COSMO-out", "COSMO-ion", and "COSMO-ion-out". In the first, the values predefined in Turbomole 7.5.1 were selected for all parameters, thus it is just called "COSMO". In COSMO-out, the outlying charge correction[67] additionally applied (see ESI for more details). In COSMO-ion,[68] the "ions" keyword is set. It changes the scaling factor $f(\varepsilon)$ to describe charged species better. The results are more similar[68] to those of the integral equation formalism with polarizable continuum model (IEFPCM).[69,70] In COSMO-ion-out equation (S2) and the outlying charge correction is applied.

Three different variants and settings of the DCOSMO-RS solvation model[71] were tested, referred here as "DCOSMORS", "DCOSMORS-out", and "DCOSMORS-out-c". Again, in the first, the values predefined in Turbomole 7.5.1 were selected for all parameters. The second also applies the outlying charge correction. In the last one, the combinatorial term[71] is added in addition to the outlying charge correction. Furthermore, the IEFPCM and the Solvation Model based on Density (SMD)[72] were tested.

The structure optimizations were performed employing all the different solvent models and settings. The only exceptions represent calculations that include the outlying charge correction and combinatorial term. Both are performed with the converged SCF cycle of the corresponding COSMO or DCOSMO-RS calculations.

Calculations with solvent models IEFPCM or SMD were performed with the Gaussian 16 C.01 software package.[39] The B3LYP implementation in Gaussian 16 C.01 uses the VWN3 functional, whereas Turbomole 7.5.1 uses the VWN5 functional.[42] For comparison, calculations were performed with the Turbomole 7.5.1 software package at B3LYP-D3(BJ)/def2-TZVP (COSMO) level of theory, utilizing the VWN3 instead of the VWN5 functional. For more details on the calculations with the solvent models, see ESI.

In addition to calculations using B3LYP DF, structure optimizations and energy calculations were carried out with 26 other DFs: LDA [=SVWN(V)],[40–42] BHLYP-D3(BJ),[73] CAM-B3LYP-D3(BJ),[74] B2PLYP-D3(BJ),[75] BP86-D3(BJ),[76] PBE-D3(BJ),[77,78] PBE0-D3(BJ),[79] TPSS-D3(BJ),[80] TPSSh-D3(BJ),[81] PW6B95-D3(BJ),[82] M06-L,[83] M06,[83] M06-2X,[83] M08-HX,[84] M11-L,[85] M11,[86] revM11,[87] MN12-L,[88] MN12-SX,[89] MN15-L,[90] MN15,[91] r2SCAN-D4 (see ESI for radial grid size of SCAN DFs),[92] SCAN-D3(BJ),[93] SCAN0,[94] wB97X,[95] and wB97XD.[96] Def2-TZVP was employed as the basis set. In addition, some DFs were used with smaller basis sets for faster prescreening steps: PBEh-3c/def2-mSVP[97] and r2SACN-3c/mTZVPP,[98] B3LYP-D3(BJ)$^+$/def2-SVP,[99] B3LYP-D3(BJ)$^-$/def2-SVP, PBE0-D3(BJ)/def2-SVP,[100] PBE0-D3(BJ)$^+$/def2-SVP, and PBE0-D3(BJ)$^-$/def2-SVP. We parametrized the B3LYP-D3(BJ)$^{+/-}$ and PBE0-D3(BJ)$^{+/-}$, see section: "Reparametrising DFs." Also HF-3c/minix[101] calculations were performed. HF-3c is wave function- and not DFT-based.

In these calculations, the solvent model COSMO was used to simulate the solvent acetonitrile. M08-HX, wB97X, and wB97XD were applied using the Gaussian 16 C.01 program package, the IEFPCM solvent model, and without the RI-approximation.

For the double-hybrid functional B2PLYP-D3(BJ), only single point calculations were performed using the structures optimized at the B3LYP-D3(BJ)/def2TZVP (COSMO) level of theory.

Reparametrizing DFs

The terms B3LYP-D3(BJ)$^+$ and PBE0-D3(BJ)$^+$ are used to describe B3LYP-D3(BJ) and PBE0-D3(BJ) DFs that use a different exact Hartree-Fock exchange E_x^{Exact} than the original version of these DFs. Equations (1) and (2) show the different contributions to these DFs.[100]

$$E_{xc}^{B3LYP} = (1-c)\,E_x^{S} + 0.72\,E_x^{B88} + 0.81\,E_c^{LYP} + 0.19\,E_c^{VWN} + c\,E_x^{Exact} \quad (1)$$

$$E_{xc}^{PBE0} = (1-c)\,E_x^{PBE} + E_c^{PBE} + c\,E_x^{Exact} \quad (2)$$

E_x^S is the Slater exchange,[41] E_x^{B88} is gradient correction to the local spin density approximation for exchange from Becke,[43] E_c^{LYP} and E_c^{VWN} are both correlation functionals.[42,44] E_x^{PBE} and E_c^{PBE} are PBE exchange and correlation functional contributions,[79] respectively. In both Equations, (1) and (2), c gives the amount of E_x^{Exact}.

The amount of exact exchange c was changed from 5% ($c = 0.05$) to 50% ($c = 0.5$) in steps of 1% ($c = 0.01$). For each step, a structural optimization was performed for the **1-X-R** radicals with X═O, R═Me, Bn; and X═S, R═Me, X═NH, and R═Me (see Scheme 2). The oxidation potential was then calculated from $E_{HOMO}^{Radical}$ using Equation (8), see section "Redox Potentials from HOMO energies." The calculated oxidation potentials were compared with the experimental oxidation potential. This is a reasonable comparison. We showed for X═O that these experimental results are almost identical to oxidation and reduction potential calculated with CCSD(T) in the basis set limit (see the results section "Wave function-based methods"). The calculated oxidation potentials closest above and below the experimental value were selected. These two potential values were plotted against their E_x^{Exact}. In this way, the value c of E_x^{Exact} at which the calculated and experimental oxidation potentials coincide could be linearly interpolated (see ESI). c was calculated for each molecule individually. Finally, the average amount of c was taken as the amount of the exact exchange E_x^{Exact} for B3LYP-D3(BJ)$^+$. The amount c of the exact exchange E_x^{Exact} for PBE0$^+$ was determined in the same way.

Similarly, the optimal amount c of exact exchange E_x^{Exact} was determined for B3LYP-D3(BJ) and PBE0-D3(BJ) to calculate the reduction potential from the E_{HOMO}^{Anion} using Equation (10), see section Redox Potentials from HOMO energies. The experimental reduction potentials for the **1-X-R** radicals with X═O, R═Me, Bn; and X═S, R═Me (see Scheme 2) served as reference date. To distinguish them from B3LYP-D3(BJ)$^+$ and PBE0-D3(BJ)$^+$, they are here referred to as B3LYP-D3(BJ)$^-$ and PBE0-D3(BJ)$^-$.

Ro-vibrational contributions to the Gibbs energy and incorporating of concentration

The ro-vibrational contributions $G_{298.15\,K}^{ro-vib}$ are calculated at the B3LYP-D3(BJ)/def2-TZVP (COSMO) level of theory, even if E_{elec} is calculated with a different DF. In cases where $G_{298.15\,K}^{ro-vib}$ is calculated with BP86-D3(BJ)/def2-TZVP (COSMO), this is explicitly stated. For more details, see ESI.

2.2.3 | Wave function-based methods

Wave function-based methods were employed to calculate the oxidation and reduction potentials for **1-O-Me**. Specifically, the MP2,[102] MP2-F12,[103] CCSD(T),[104] and CCSD(T)-F12[104] methods were utilized. In addition, SCS-MP2,[105] SOS-MP2,[106] and CCSD[104] were

used. RI approximations were applied in all cases. The radical species had to be calculated with ROHF, as the unrestricted Hartree-Fock (UHF) calculations suffered from spin-contamination. The oxidized and reduced species were calculated using the restricted Hartree-Fock (RHF) method. The starting structures were determined at the B3LYP-D3(BJ)/def2-TZVP (COSMO) level of theory as described above. For these structures, single point gas phase calculations were performed using the wave function-based methods. The basis set limit for $E_{\text{Limit}}^{\text{Corr}}$ for the correlation energies was extrapolated by an approach described by Helgaker et al. (see ESI).[107] The correlation energy for this was determined using two basis sets where the cardinal numbers differ by one. The Hartree-Fock (HF) energy was calculated with the largest basis set used in the extrapolation. See ESI for further details. In addition, the extrapolation of $E_{\text{Limit}}^{\text{Corr}}$ was done using an approach of Marshall et al.[108] The correlation energy is extrapolated on the MP2 level as before. Then the difference to CCSD(T) is added (see ESI). This approach allows even larger basis sets to be used.

The solvation energies of the cation, radical, and anion have to be added to the wave function-based results to be able to compare them with the experimental results. The solvation energy that is gained by bringing the molecule from the gas phase into solution, where the structure further relaxes, was calculated at the DFT level. Single-point calculations with B3LYP-D3(BJ)/def2-TZVP in the gas phase were performed with the same structures used for the (single-point) wave function-based calculations. The structures were then reoptimized on the B3LYP-D3(BJ)/def2-TZVP [DCOSMO-RS(acetonitrile)] level of theory. The energy difference between the gas phase and DCOSMO-RS-out (Acetonitrile) was added to the electronic energy of the molecule calculated with the wave function-based methods. The $G_{298.15\,\text{K}}^{\text{ro-vib}}$ values for the wave function-based results were calculated at the B3LYP-D3(BJ)/def2-TZVP (COSMO) level of theory.

2.2.4 | Calculations of the oxidation a reduction potentials

Redox potentials from Gibbs energies

The oxidation potentials E_{Ox} and reduction potentials E_{Red} were calculated according to the equations

$$E_{\text{Ox}} = -\frac{\Delta G_{\text{Ox}}}{nF} - E_{\text{Ag/AgNO}_3} \tag{3}$$

$$E_{\text{Red}} = -\frac{\Delta G_{\text{Red}}}{nF} - E_{\text{Ag/AgNO}_3} \tag{4}$$

with the electrode potential $E_{\text{Ag/AgNO}_3}$, the Faraday constant F, the number of electrons n in the half reaction, and the Gibbs energies of oxidation ΔG_{Ox} and reduction ΔG_{Red}. The latter are defined as:

$$\Delta G_{\text{Ox}} = G^{\circ}_{298.15\,\text{K}}(\text{radical}) - G^{\circ}_{298.15\,\text{K}}(\text{e}^-) - G^{\circ}_{298.15\,\text{K}}(\text{cation}) \tag{5}$$

$$\Delta G_{\text{Red}} = G^{\circ}_{298.15\,\text{K}}(\text{anion}) - G^{\circ}_{298.15\,\text{K}}(\text{e}^-) - G^{\circ}_{298.15\,\text{K}}(\text{radical}). \tag{6}$$

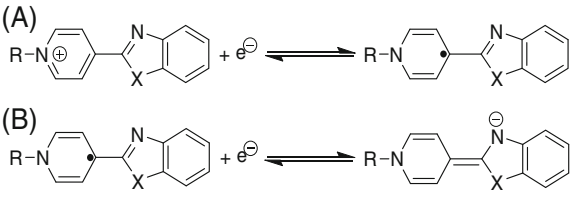

SCHEME 3 (A) Schematic representation of the oxidation reaction considered for obtaining ΔG_{Ox}, (B) reduction reaction considered for obtaining ΔG_{Red}; with X═O, S, NH; R═Me, Bn.

$G^{\circ}_{298.15\,\text{K}}(\text{e}^-) = -3.632\,\text{kJ mol}^{-1}$ is the Gibbs energy of a free electron.[26] $G^{\circ}_{298.15\,\text{K}}(\text{cation})$, $G^{\circ}_{298.15\,\text{K}}(\text{radical})$ and $G^{\circ}_{298.15\,\text{K}}(\text{anion})$ are the Gibbs energies for the oxidized, radical and reduced species, respectively, calculated at 298.15 K and $1\,\text{mol L}^{-1}$ as described in Equation (2). Scheme 3A and Scheme 3B show the corresponding reactions for ΔG_{Ox} and ΔG_{Red}.

The electrode potential $E_{\text{Ag/AgNO}_3}$ of the Ag/AgNO_3 reference electrode is calculated using Equation (7).[109]

$$E_{\text{Ag/AgNO}_3} = E_{\text{SHE}}^{\text{Vacuum}} + E_{\text{NHE}}^{\text{SHE}} + E_{\text{Ag/AgNO}_3}^{\text{NHE}} \tag{7}$$

The Ag/AgNO_3 electrode in acetonitrile has an (experimental) electrode potential of $E_{\text{Ag/AgNO}_3}^{\text{NHE}} = +0.548\,\text{V}$ versus NHE in water.[109] The difference $E_{\text{NHE}}^{\text{SHE}}$ between the NHE potential and the standard hydrogen electrode (SHE) potential is −0.006 V.[26] However, different values were proposed for the absolute electrode potential $E_{\text{SHE}}^{\text{Vacuum}}$ itself (4.05 V,[110,111] 4.11 V,[110,112] 4.21 V,[110,113] 4.28 V,[114,115] 4.34 V,[26,116] 4.42 V,[117] 4.44 V,[118] 4.47 V[26,119]). Therefore, computational solvent models were designed based on different $E_{\text{SHE}}^{\text{Vacuum}}$ values.[26] For quantum chemical calculations, $E_{\text{SHE}}^{\text{Vacuum}} = 4.28\,\text{V}$ is commonly used today.[120] This $E_{\text{SHE}}^{\text{Vacuum}}$ value is also used in the presented study, and gives $E_{\text{Ag/AgNO}_3} = 4.822\,\text{V}$. This value was used for all calculations, except those using the IEFPCM solvent model. IEFPCM was parameterized with $E_{\text{SHE}}^{\text{Vacuum}} = 4.47\,\text{V}$. This gives $E_{\text{Ag/AgNO}_3} = 5.012\,\text{V}$, which was used here for calculations with the IEFPCM solvent model.

Redox potentials from electronic energies

The Gibbs energies of oxidation ΔG_{Ox} and reduction ΔG_{Red} can be approximated by neglecting $G_{298.15\,\text{K}}^{\text{ro-vib}}$ [see equation (S4) in ESI]. The electronic energy E_{elec} is then the only term to be calculated quantum mechanically. This allows a much faster calculation of the oxidation and reduction potentials using Equations (3)–(6).

Redox potentials from HOMO energies

The oxidation potential can be estimated from the energy of the highest occupied orbital (HOMO) of the radical $E_{\text{HOMO}}^{\text{Radical}}$.

$$E_{\mathrm{Ox}}^{\mathrm{HOMO}} = \frac{-E_{\mathrm{HOMO}}^{\mathrm{Radical}}}{nF} - E_{\mathrm{Ag/AgNO_3}}. \quad (8)$$

Similarly, the reduction potential can be estimated from the energy of the LUMO of the radical $E_{\mathrm{LUMO}}^{\mathrm{Radical}}$

$$E_{\mathrm{Red}}^{\mathrm{LUMO}} = \frac{-E_{\mathrm{LUMO}}^{\mathrm{Radical}}}{nF} - E_{\mathrm{Ag/AgNO_3}}. \quad (9)$$

Furthermore, the reduction potential can also be estimated from the energy of the HOMO of the reduced species $E_{\mathrm{HOMO}}^{\mathrm{Anion}}$

$$E_{\mathrm{Red}}^{\mathrm{HOMO}} = \frac{-E_{\mathrm{HOMO}}^{\mathrm{Anion}}}{nF} - E_{\mathrm{Ag/AgNO_3}}. \quad (10)$$

Quantification of the deviation between calculation and experiment

Δ_{Ox}, Δ_{Red}, Δ_{Avg}, $\Delta_{\mathrm{Ox-HOMO}}$, $\Delta_{\mathrm{Red-LUMO}}$, $\Delta_{\mathrm{Red-HOMO}}$, $\Delta_{\mathrm{Ox}}^{\mathrm{CCSD(T)}}$, $\Delta_{\mathrm{Red}}^{\mathrm{CCSD(T)}}$, $\Delta_{\mathrm{Avg}}^{\mathrm{CCSD(T)}}$, $\Delta_{\mathrm{Ox-HOMO}}^{\mathrm{CCSD(T)}}$, $\Delta_{\mathrm{Red-LUMO}}^{\mathrm{CCSD(T)}}$, and $\Delta_{\mathrm{Red-HOMO}}^{\mathrm{CCSD(T)}}$ are defined to quantify the deviation between the calculated and reference [experimental or CCSD(T)] oxidation and reduction potentials, respectively. For more details see ESI.

3 | RESULTS AND DISCUSSION

3.1 | Method assessment

As a first step, an in-depth method evaluation is performed for **1-O-Me**. The results of this were used in the second part of this study to design the multistep screening approach. The equilibrium structures were determined with a conformer search, as described in the computational details. These structures were used as starting structures for all other methods. The structures are shown in the electronic supplementary information (ESI) together with the EPMs (Figure S1).

3.1.1 | Wavefunction-based methods

Figure 1 shows the oxidation and reduction potentials of **1-O-Me** calculated with MP2, MP2-F12, CCSD(T) and CCSD(T)-F12 in conjunction with the def2-XVPD (X=S, TZ), (aug-)cc-pVXZ (X=D, T, Q, 5) and cc-pXVZ-F12 (X=D, T, Q) basis sets. Results with additional basis sets [def2-XVP (X=S, TZ, QZ), def2-TZVPP, def2-XVPPD (X=TZ, QZ)], methods (SCS-MP2, SOS-MP2, CCSD) and deviations (Δ_{Ox}, Δ_{Red}, Δ_{Avg}) to the experimental results are shown in Figures S4–S6. These calculations were performed as single point calculations. Solvation effects are taken into account using the DCOSMO-RS-out solvent model. It was used because it includes physically meaningful contributions such as hydrogen bonds.

As expected, all methods underestimate the oxidation and reduction potentials when used with small basis sets (Figures 1 and S4–S6). As the basis set is increased, the calculations approach the experimental oxidation and reduction potentials. At the basis set limit cbs(aug-cc-pVQZ→aug-cc-pV5Z) [abbreviated as cbs(Q→aV5Z)], extrapolated from the largest applied basis sets, MP2 overestimates the oxidation potential by only 0.01 V and underestimates the reduction potential by 0.09 V. Using diffuse functions for the basis set limit MP2/cbs (Q→aV5Z) provides an improvement of 0.02 V for the reduction potential compared to MP2/cbs(Q→V5Z) without diffuse functions.

MP2-F12 with the largest F12 basis set (cc-pVQZ-F12) gives the same accuracy as MP2 without F12 in the basis set limit cbs(Q→V5Z), but about four times faster. SCS- and SOS-MP2 are discussed in the ESI, but they do not improve the Δ_{Avg} compared to MP2.

The oxidation and reduction potentials calculated at the CCSD(T) basis set limit, CCSD(T)/cbs(S→TZVPD), have an average deviation from the experiment of only 0.02 V ($\Delta_{\mathrm{Ox}} = 0.00$ V, $\Delta_{\mathrm{Red}} = 0.04$ V, $\Delta_{\mathrm{Avg}} = 0.02$ V). CCSD(T)-F12/cc-pVDZ-F12 has an equally small deviation ($\Delta_{\mathrm{Ox}} = 0.01$ V, $\Delta_{\mathrm{Red}} = 0.03$ V, $\Delta_{\mathrm{Avg}} = 0.02$ V). The CCSD(T)/cbs (S→TZVPD) and the experimental oxidation potential are the same, meaning $\Delta_{\mathrm{Ox}} = 0.00$ V. The reduction potential calculated at the CCSD(T)/cbs(S→TZVPD) level of theory is closer to the experiment than all MP2 calculations. The choice of Ahlrich's def2-type basis sets over Dunning's correlation consistent basis sets for the CCSD(T) calculations is explained in the ESI.

To extrapolate the basis set limit from a larger basis set, we employed an approach investigated by Marshall[108]: CCSD(T)/cbs (Q→aV5Z)* adds the difference between CCSD(T) and MP2 for the def2-TZVPD basis set to the MP2/cbs(Q→aV5Z) correlation energy. With this approach, the oxidation and reduction potentials get both slightly overestimated ($\Delta_{\mathrm{Ox}} = -0.06$ V, $\Delta_{\mathrm{Red}} = -0.03$ V, $\Delta_{\mathrm{Avg}} = 0.05$ V) but this result should be the most accurate prediction of the CCSD(T) basis set limit. The slightly larger deviation ($\Delta_{\mathrm{Avg}} = 0.05$ V) compared to the CCSD(T) calculations with smaller basis set could be due to the potential $E_{\mathrm{Ag/AgNO_3}}$ for the $Ag/AgNO_3$ reference electrode or the solvation model.

The CCSD(T)/cbs(Q→aV5Z)* level's overestimation may be attributed to selecting $E_{\mathrm{SHE}}^{\mathrm{Vacuum}} = 4.28$ V to determine the $Ag/AgNO_3$ reference electrode potential. Further discussion of this issue is provided in the ESI. The ESI also includes an analysis of the potential multireference nature of the systems under investigation.

In summary, the experiment and the high-level wave function-based approach are in excellent agreement. The small deviations may be due to the fact that the absolute potential of the SHE $E_{\mathrm{SHE}}^{\mathrm{Vacuum}}$ for the solvent model is not well known, to the limited accuracy of the solvent model itself, or to experimental factors. In the following the experimental and CCSD(T)/cbs(Q→aV5Z)* results will be used for the evaluation of the DFs.

3.1.2 | DFT: Dispersion corrections, basis sets, solvent models, and DFs

The next step was to test different dispersion corrections, basis sets, solvent models, and DFs by calculating the oxidation and reduction potential of **1-O-Me**. The structures of the differently charged **1-O-Me** species were reoptimized and their electronic energies were calculated with all

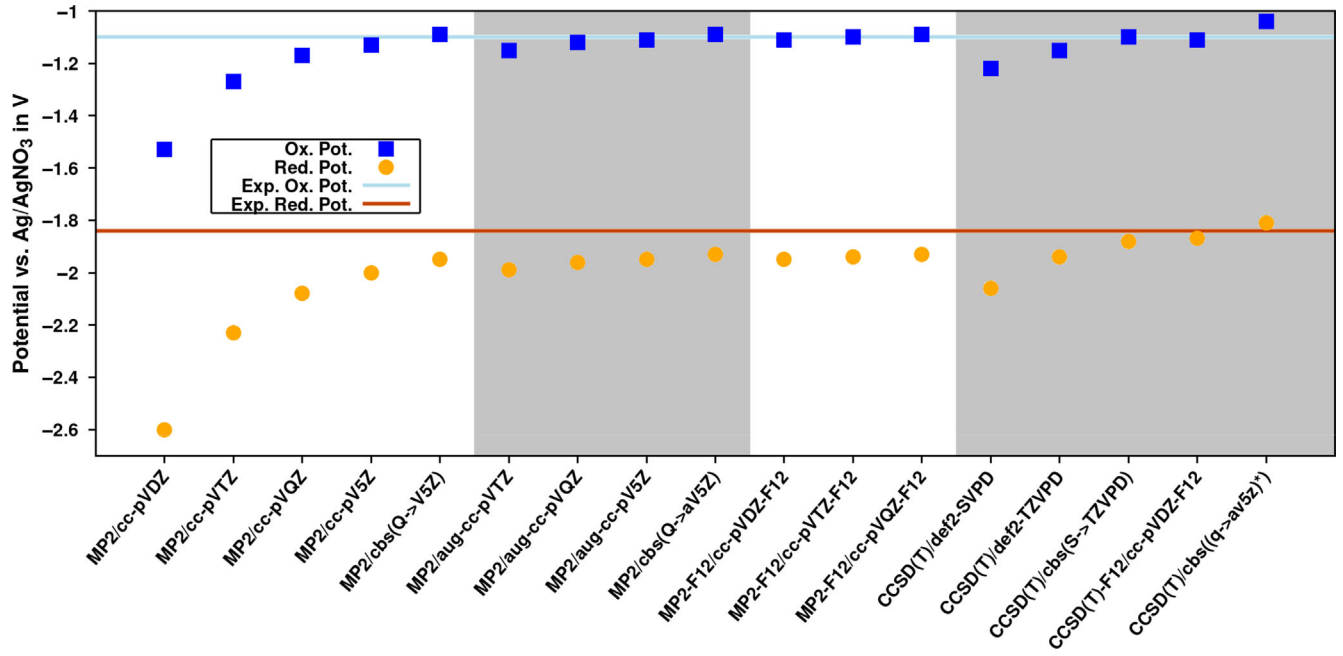

FIGURE 1 E_{Ox} and E_{Red} of **1-O-Me** calculated with different wave function-based methods. The solvent effects have been calculated with the DCOSMO-RS-out model at the B3LYP-D3(BJ)/def2-TZVP level of theory. The oxidation potential E_{Ox} is shown as blue filled boxes (calculated values), and light blue line (experimental value). The reduction potential E_{Red} is displayed as orange filled circles (calculated values), and dark orange line (experimental value).

these methods. The ro-vibrational contributions were calculated on the B3LYP-D3(BJ)/def2-TZVP (COSMO) level of theory in all cases.

B3LYP, basis functions, and dispersion correction

First, B3LYP-D3(BJ) with the COSMO solvation model was used with different sized Ahlrich's def2-type basis sets. The results are shown in Figures 2 and S7 in comparison with the experimental and the CCSD(T)/cbs(Q→aV5Z)* results.

B3LYP combined with all basis sets underestimates the experimental oxidation and reduction potentials. Consequently, the deviation from the CCSD(T)/cbs(Q→aV5Z)* benchmark values is even slightly larger. Moreover, the deviation Δ_{Red} of the calculated reduction potential from the experimental value is three to four times larger than the corresponding deviation Δ_{Ox} for the oxidation potentials.

Surprisingly, the def2-SVPD basis set leads to the smallest deviations ($\Delta_{Avg} = 0.23\,V$). A comparison of the total energies indicates that the def2-SVPD basis set probably adds disproportionately many basis functions to describe electrons further away from the nuclei. As a result, the anion is stabilized too much and the cation too little. Thus, the good agreement with def2-SVPD is probably based on unreliable error cancellation. Not taking into account def2-SVPD, increasing the basis set always improves here the agreement with the experimental values. The largest basis set tested is def2-QZVPPD ($\Delta_{Ox} = 0.13\,V, \Delta_{Red} = 0.38\,V, \Delta_{Avg} = 0.25\,V$). The deviations with the def2-TZVP basis set ($\Delta_{Ox} = 0.15\,V, \Delta_{Red} = 0.42\,V, \Delta_{Avg} = 0.29\,V$) are close to the deviations with the basis set def2-QZVPPD($\Delta_{Avg} = 0.25\,V$). In addition, the structural differences between the def2-TZVP and

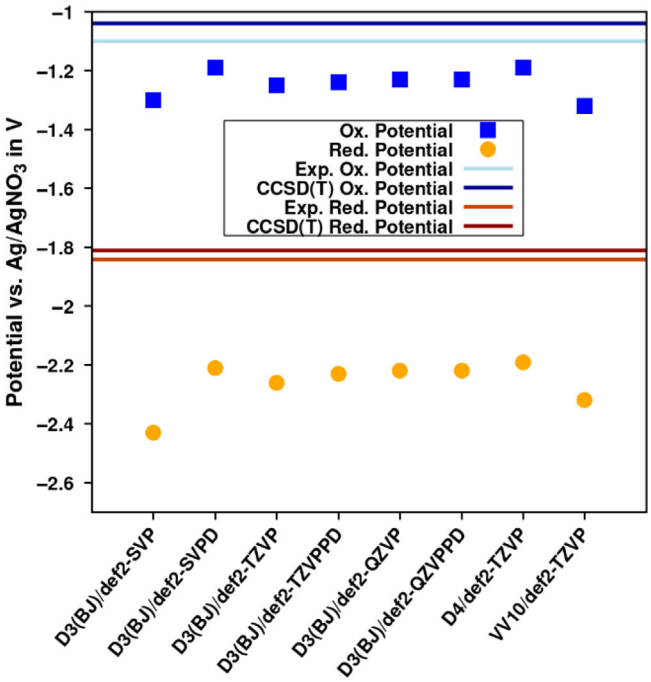

FIGURE 2 E_{Ox} and E_{Red} of **1-O-Me** calculated with B3LYP and COSMO. The basis set and dispersion correction have been varied. The oxidation potential E_{Ox} is shown as blue filled boxes (calculated with DFT), light blue line (experimental value) and dark blue line [CCSD(T)/cbs(Q→aV5Z)*]. The reduction potential E_{Red} is shown as orange filled circles (calculated with DFT), dark orange line (experimental value), and brown line [CCSD(T)/cbs (Q→aV5Z)*].

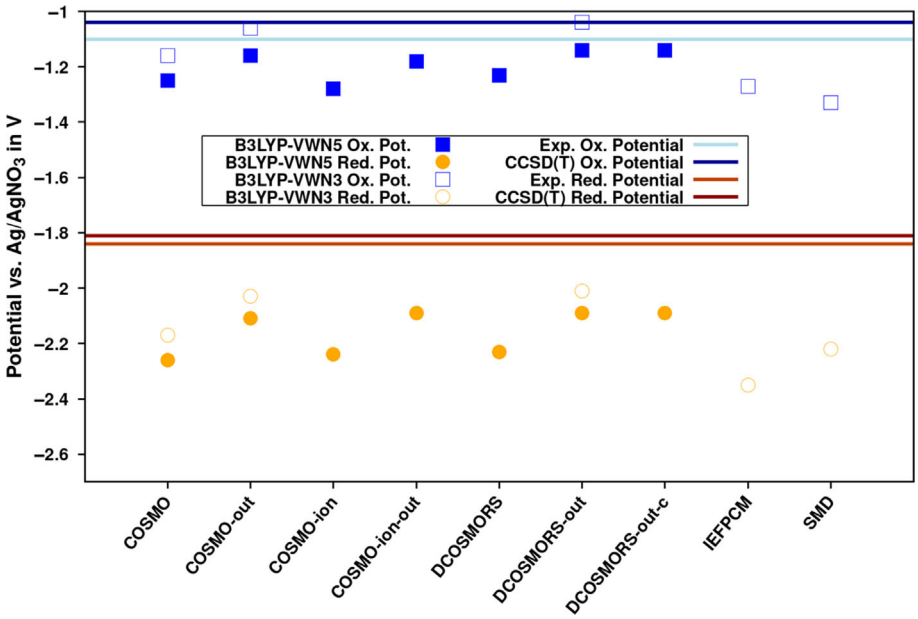

FIGURE 3 E_{Ox} and E_{Red} of **1-O-Me** calculated with B3LYP-D3(BJ)/def2-TZVP. The solvent model was varied. The B3LYP DF was utilized with the VWN3 and the VWN5 correlation functional. When VWN5 was utilized, the $\varepsilon_r = 37.5$ was applied. VWN3 was employed with $\varepsilon_r = 35.688$. The oxidation Potential E_{Ox} is displayed as blue filled boxes (B3LYP utilizing VWN5), blue empty boxes (B3LYP utilizing VWN3), light blue line (experimental value), and dark blue line [CCSD(T)/cbs(Q→aV5Z)*]. The reduction potential E_{Red} is shown as orange filled circles (B3LYP utilizing VWN5), orange empty circles (B3LYP utilizing VWN3), dark orange line (experimental value), and brown line [CCSD(T)/cbs(Q→aV5Z)*].

def2-QZVPPD optimized structures are very small, see Table S1 in the ESI. Thus, def2-TZVP is sufficient for structure optimization and calculating the energies.

The dispersion corrections D4 and VV10 were also tested (Figure 2). In contrast to D3(BJ), both take into account the charge of the system. Therefore, both should improve the agreement with the experimental and the CCSD(T)/cbs(Q→aV5Z)* benchmark potentials. Surprisingly, the use of VV10 leads to larger deviations ($\Delta_{Avg} = 0.35$ V) than D3(BJ).

D4 improves the agreement with the experimental oxidation and reduction potential by 0.06 and 0.07 V, respectively. This is a larger effect than the differences between def2-TZVP and def2-QZVPPD basis sets. The structures deviate on average by 0.3 to 0.8 p.m. (Table S1) compared to D3(BJ), which is smaller than the structural changes due to the use of the basis set def2-TZVP. However, when D4 is employed, it cannot be expected to meet very tight convergence criteria for energy and gradients in every case.[36] This is because the D4 gradient calculations use an approximation (the Axilrod-Teller-Muto three-body term).[36,62] The methods presented here are intended to be used for screening large numbers of molecules and calculating vibrational frequencies. Therefore, the more stable D3(BJ) method is used in the following.

Overall, the dispersion correction D3(BJ) and the basis set def2-TZVP provide structures close to the improved dispersion correction D4 and the basis set limit (see Table S1 for RMSD values). The use of D3(BJ) together with def2-TZVP leads to an underestimation of the oxidation and reduction potential by 0.08 and 0.11 V compared to employing D4 and def2-QZVVPD.

B3LYP and solvent model

In this section, the performance of different implicit solvent models for DFT is assessed. The results are shown in Figure 3. Figure S8 includes values for the deviations Δ_{Ox}, Δ_{Red}, and Δ_{Avg} to the experiment. The COSMO, and COSMO-ion have the largest deviation ($\Delta_{Avg} = 0.29$ V) from the experimental oxidation and reduction potentials.

The largest improvement compared to the COSMO is achieved by including the outlying charge correction (COMSO-out; $\Delta_{Avg} = 0.17$ V). This improves the agreement with the experimental oxidation and reduction potential by 0.09 and 0.15 V, respectively. The COSMO-ion is intended to improve the description of charged species. However, it improves the agreement with the experimental reduction potential as much as it worsens the agreement to experimental oxidation potential (0.02 V). The reason for this is that the charged species are both stabilized while the energy of radical species remains the same. The COSMO-ion is supposed to bring results closer to the results of the IEFPCM solvent model.[68] This is not noticed here because COSMO and IEFPCM use different atom radii and cavities types (solvent excluded surface versus van der Waals surface).

COSMO-ion-out differs from COSMO-out in the same way as COSMO-ion from COSMO. The DCOSMO-RS model includes additional interactions into the COSMO model (see ESI). It improves the agreement with the experimental oxidation and reduction potentials by 0.02 and 0.03 V, respectively. Adding the outlying charge correction to DCOSMO-RS (i.e., DCOSMO-RS-out) gives the same improvement as for COSMO. Including the combinatorial term (DCOSMORS-out-c) has no effect on the oxidation and reduction potential, the deviations (Δ_{Ox}, Δ_{Red}, Δ_{Avg}) remain the same. In all these cases, the calculation underestimated the experimental oxidation and reduction potentials. Accordingly, B3LYP-D3(BJ)/def2-TZVP underestimates the CCSD(T)/cbs(Q→aV5Z)* potentials even more with all COSMO and DCOSMO-RS variants.

The IEFPCM and SMD model had to be calculated with B3LYP utilizing the VWN3 instead of the VWN5 functional and a slightly different relative primitivity. The change in relative permittivity had basically no effect on oxidation and reduction potentials see ESI. Switching from VWN5 to VWN3 for B3LYP-D3(BJ)/def2-TZVP (COSMO) improves agreement with the experimental

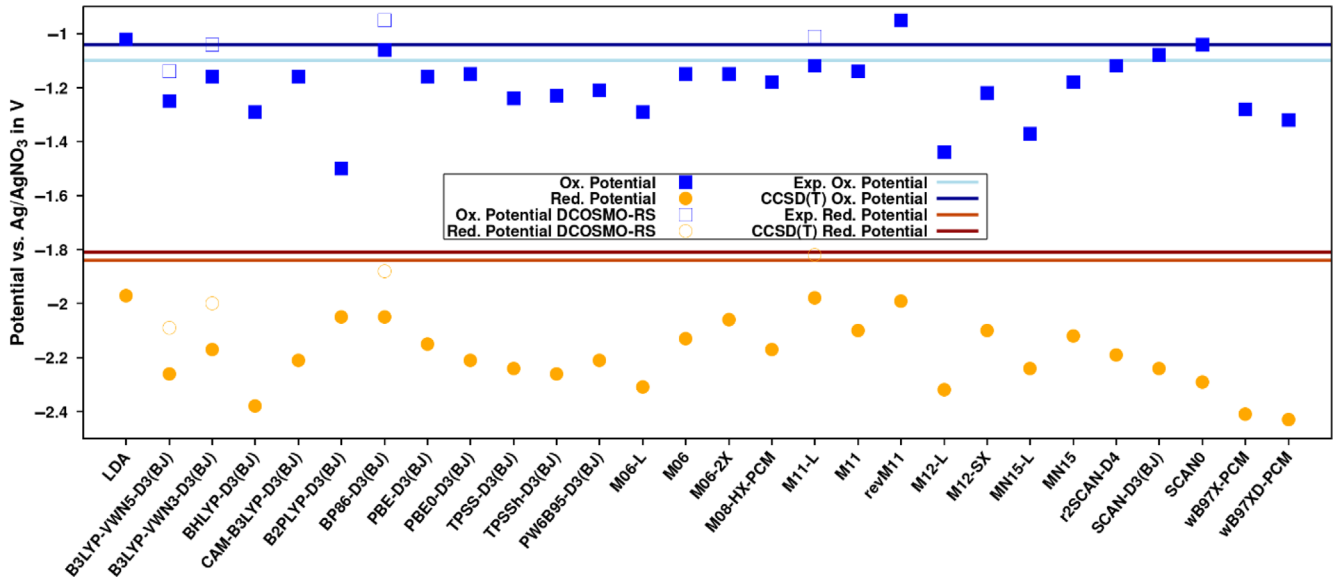

FIGURE 4 E_{Ox} and E_{Red} of **1-O-Me** calculated with different DFs and the basis set def2-TZVP. The solvent effects are included with COSMO. The exceptions are M08-HX, wB97X, and wB97XD, for which the IEFPCM solvent model was used (which is indicated by the suffix -PCM). For B3LYP-D3(BJ) with VWN5 and VWN3, BP86-D3(BJ) and M11-L, the results with the DCOMOS-RS-out solvent model are also given. The oxidation potential E_{Ox} is displayed as blue filled boxes (DFs with COSMO or IEFPCM), blue empty boxes (DFs with DCOSMO-RS), light blue line (experimental value), and dark blue line [CCSD(T)/cbs(Q→aV5Z)*]. The reduction potential E_{Red} is shown as orange filled circles (DFs with COSMO or IEFPCM), orange empty circles (DFs with DCOSMO-RS), dark orange line (experimental value), and brown line [CCSD(T)/cbs (Q→aV5Z)*].

oxidation and reduction potential by 0.09 V each ($\Delta_{Ox} = 0.06$ V, $\Delta_{Red} = 0.33$ V, $\Delta_{Avg} = 0.19$ V). Similarly, the deviations of COSMO-out, and DCOSMO-RS-out improve by switching from VWN5 to VWN3.

Despite the usage of the VWN3 functional, the IEFPCM model has the highest deviations ($\Delta_{Ox} = 0.17$ V, $\Delta_{Red} = 0.51$ V, $\Delta_{Avg} = 0.34$ V) of all tested solvent models DF combinations in Figure 3. The COSMO and IEFPCM methods are fairly similar, except the cavity construction.[121] Therefore, the better agreement for COSMO indicates that the COSMO solvent models (that includes DCOSMO-RS) constructs better cavities for the systems of interested. On average, SMD ($\Delta_{Ox} = 0.23$ V, $\Delta_{Red} = 0.38$ V, $\Delta_{Avg} = 0.30$ V) improves upon the IEFPCM model, but still has larger deviations from the experimental and CCSD(T)/cbs(Q→aV5Z)* results than the COSMO-based solvation models.

In total, the solvent model that archives the best agreement with the experimental and CCSD(T)/cbs(Q→aV5Z)* oxidation and reduction potential is DCOSMO-RS-out. In contrast to the COSMO and IEFPCM model, the DCOSMO-RS-out includes hydrogen bonds to the solvent, and in contrast to IEFPCM and SMD it accounts for the electron density outside the cavity. In addition with good agreement to the experimental results, this makes DCOSMO-RS-out the ideal model for the CCSD(T)/cbs(Q→aV5Z)* reference values.

For the reduction potential, B3LYP-D3(BJ)/def2-TZVP (DCOSMO-RS-out) has still a large deviation to the experimental and CCSD(T)/cbs(Q→aV5Z)* reference value. Therefore, different DFs are tested in the next step for the calculation of the oxidation and reduction potential.

DFT functionals

This section tests the performance of 27 different DFs. The selected functionals include LDA, GGA, meta-GAA, hybrid (meta-)GGA, range-separate hybrid (meta-)GGA, double-Hybrid GGA, empirical, and nonempirical functionals. This covers all commonly used density functional types. In all cases, the def2-TZVP basis set is employed. Unless otherwise stated, the COSMO solvation model is used. The results for the oxidation and reduction potentials are shown in Figure 4, and the deviations in Figure S9. Most DFs underestimate the experimental oxidation and reduction potentials.

The meta-GGA M11-L has the highest agreement with the experiment ($\Delta_{Ox} = 0.02$ V, $\Delta_{Red} = 0.14$ V, $\Delta_{Avg} = 0.08$ V). Its hybrid variant M11 is the DF with the fifth highest agreement with the experiment ($\Delta_{Ox} = 0.04$ V, $\Delta_{Red} = 0.26$ V, $\Delta_{Avg} = 0.15$ V). Thus, the DF which on a lower rung (M11-L) of the Jacobs Ladder[122] agrees better than its higher rung variant (M11). The successor of the M11-L DF in the Minnesota DF family, MN15-L, belongs to the DFs with the lowest agreement with the experiment ($\Delta_{Ox} = 0.27$ V, $\Delta_{Red} = 0.40$ V, $\Delta_{Avg} = 0.33$ V). Method evaluations by Q. Zhang et al.[24] and W. Zhang et al.[28] show that the M08-HX DF predicts redox potentials the best. Their test systems were on quinones and common solvents for Li batteries, respectively. Here, M08-HX performs average ($\Delta_{Ox} = 0.08$ V, $\Delta_{Red} = 0.33$ V, $\Delta_{Avg} = 0.20$ V). It was used by us in conjunction with the IEFPCM model. The results above revealed that the IEFPCM model performs not as good as COSMO, which was used for most of the other DFs in the presented study. The use of different solvent models may explain why the presented results do not agree with these previous method evaluations.[24,28]

Surprisingly, the DF with the second highest agreement with the experiment is the LDA functional SVWN ($\Delta_{Ox} = -0.08$ V, $\Delta_{Red} = 0.13$ V, $\Delta_{Avg} = 0.11$ V). One reason for the good performance could be that the three species have almost the same structure. Errors due to the inhomogeneity of the electron density are likely to cancel each other out. However, the methyl group is not as much moved out of plane in the reduced species as for the other DFs (see Table S2). The GGA DF BP86-D3(BJ) has the third highest agreement with the experimental values of redox potentials ($\Delta_{Ox} = -0.04$ V, $\Delta_{Red} = 0.21$ V, $\Delta_{Avg} = 0.12$ V). The GGA DFs exhibit in most cases better agreement with the experiment than their hybrid variant, and the three DFs with highest agreement are all GGA density functionals. However, the DF with the lowest agreement is also a GGA DF (MN12-L). In summary, the results show no correlation between the type of DF and the agreement with the experimental results of the redox potentials.

The DFs reveal similar agreement with the CCSD(T)/cbs (Q→aV5Z)* results as with the experimental values. However, the agreement is usually a little lower. The CCSD(T)/cbs(Q→aV5Z)* oxidation and reduction potentials are slightly higher than the experimental ones, and most DFs already underestimate the experimental potentials. The order of which DFs agree best changes slightly. The best agreement to the CCSD(T)/cbs(Q→aV5Z)* results has the LDA functional SVWN $\left(\Delta_{Avg}^{CCSD(T)} = 0.09\,V\right)$. M11-L has the second highest agreement $\left(\Delta_{Avg}^{CCSD(T)} = 0.12\,V\right)$ and BP86-D3(BJ) again has the third highest $\left(\Delta_{Avg}^{CCSD(T)} = 0.13\,V\right)$.

There are two other comparisons of DFs with benchmark values, we would like to point out. First, the double-hybrid functional B2PYLP-D3(BJ) is one of the DFs with the lowest agreement with the experiment ($\Delta_{Ox} = 0.40$ V, $\Delta_{Red} = 0.20$ V, $\Delta_{Avg} = 0.31$ V). For the oxidation potential, it has the lowest agreement for of all DFs [to the experimental values and CCSD(T)/cbs(Q→aV5Z)*]. Second, the relatively new SCAN DF family performs average compared to the other DFs, with r2SCAN-D4 ($\Delta_{Avg} = 0.18$ V) performing the best out of the three tested.

The previous section demonstrated that of all the solvent models tested, DCOSMO-RS-out gave the best agreement with the experimental results. Furthermore, the solvent effects for the CCSD(T)/cbs (Q→aV5Z)* were also calculated with this solvent model. We therefore applied the DCOSMO-RS-out solvent model to the best performing DFs: M11-L and BP86-D3(BJ). We did not consider LDA, because of the structural deviations of the anion compared to all other DFs (Table S2). For both, M11-L and BP86-D3(BJ), the agreement with the experimental and the CCSD(T)/cbs(Q→aV5Z)* oxidation and reduction potentials increases. M11-L results have the highest agreement $\left(\Delta_{Avg} = 0.05\,V, \Delta_{Avg}^{CCSD(T)} = 0.02\,V\right)$ and are almost identical to the CCSD(T)/cbs(Q→aV5Z)* results. In case of BP86-D3(BJ), the reduction potential is much closer to the experimental value ($\Delta_{Red} = 0.04$ V). The oxidation potential increases but was already too high for BP86-D3(BJ) (COSMO). Accordingly, the agreement is reduced($\Delta_{Ox} = -0.15$ V). Nevertheless, the average deviation to the experiment is still reduced by 0.02 V and to the CCSD(T)/cbs (Q→aV5Z)* results by 0.05 V, $\left(\Delta_{Avg} = 0.10\,V, \Delta_{Avg}^{CCSD(T)} = 0.08\,V\right)$.

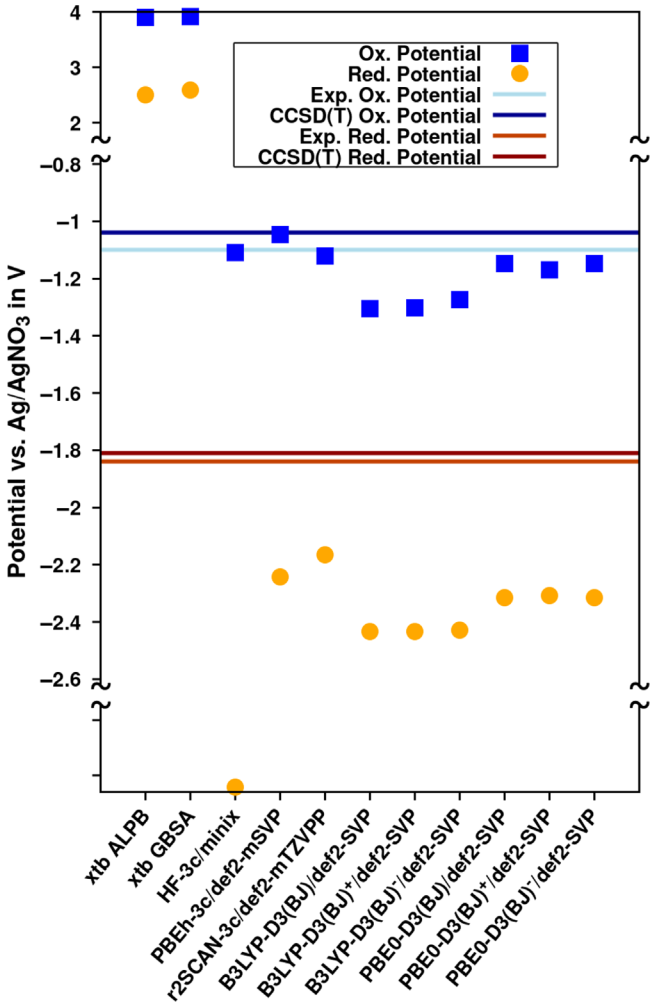

FIGURE 5 E_{Ox} and E_{Red} of **1-O-Me** calculated with different semi-empirical methods, Hartree-Fock, and DFT. The solvent effects were included with COSMO solvent model. The exception is xTB, which was carried out with GFN2-xTB and the solvent models ALPB and GBSA. The oxidation potential E_{Ox} is displayed as blue filled boxes (calculated value), light blue line (experimental value), and dark blue line [CCSD(T)/cbs(Q→aV5Z)*]. The reduction potential E_{Red} is shown as orange filled circles (calculated value), dark orange line (experimental value), and brown line [CCSD(T)/cbs(Q→aV5Z)*].

In addition, to the DFs, we tested methods that are designed for fast calculations. These are Hatree-Fock and DFT-based methods optimized for use with smaller basis sets: HF-3c/minix, PBEh-3c/def2-mSVP, and r2SCAN-3c/def2-mTZVPP. The solvent effects were again modeled with the COSMO. The oxidation and reduction potentials are shown in Figure 5, and the deviations in Figure S10. HF-3c predicts the oxidation potential almost perfectly ($\Delta_{Ox} = 0.01$ V), but has a large deviation of $\Delta_{Red} = 3.37$ V for the reduction potential. A reason for this could be that the minimal basis set minix does not provide adequate basis functions for the outlying charge of the reduced species. PBEh-3c ($\Delta_{Avg} = 0.23$ V) and r2SCAN-3c ($\Delta_{Avg} = 0.17$ V) perform averagely compared to the other DFs (Figure 4). Despite the

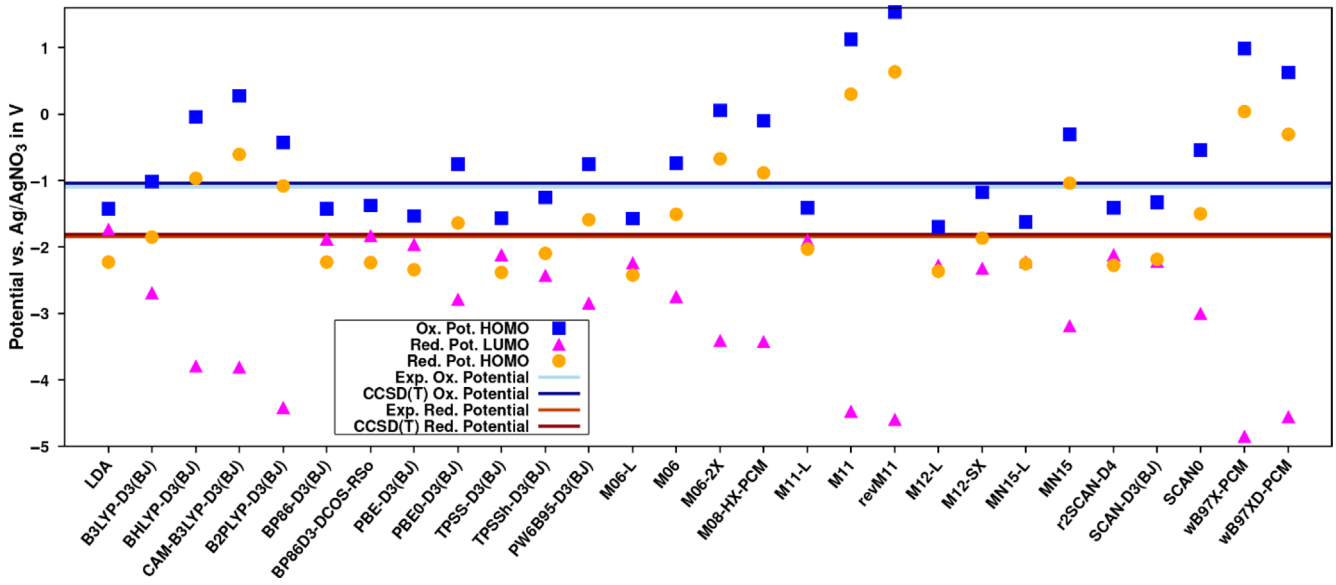

FIGURE 6 E_{Ox} and E_{Red} of **1-O-Me** estimated from the orbital energies. Different DFs have been used with the def2-TZVP basis set. The solvent effects were usually included with COSMO. The exception is BP86D3-DCOS-RSo, which is the BP86-D3(BJ) DF with the DCOSMO-RS-out solvent model. Furthermore, M08-HX-PCM, wB97X-PCM and wB97XD-PCM utilize the IEFPCM model instead of COSMO. The oxidation potential E_{Ox} is displayed as blue filled boxes (calculated from the HOMO of the radical), light blue line (experimental value) and dark blue line [CCSD(T)/cbs(Q→aV5Z)*]. The reduction potential E_{Red} is shown as purple filled triangles (calculated from the LUMO of the radical), orange filled circles (calculated from the HOMO of the anion), dark orange line (experimental value), and brown line [CCSD(T)/cbs(Q→aV5Z)*].

smaller basis set, r2SCAN-3c/def2-mTZVPP performs slightly better than r2SCAN/def2-TZVP ($\Delta_{Avg} = 0.18$ V). We also test the semi-empirical GFN2-xTB method with the solvent models ALPB and GBSA. Both strongly overestimate the oxidation and reduction potentials by about 3.9 and 2.5 V, respectively.

Redox potentials from orbital energies

Another way to screen for oxidation and reduction potential is to analyze the orbital energies. As with Hartree-Fock, the Kohn-Sham DFT HOMO energies correspond to the ionization energy.[123] Therefore, the HOMO energies of the radical and reduced species were used to calculate the oxidation and reduction potentials using Equations (8) and (10), respectively. The advantage is that it is not necessary to calculate the oxidized species. This would reduce the number of calculations needed for the screening process by one third. The calculation of the reduced species can also be omitted if the LUMO energies of the radical species are used to calculate the reduction potential [Equation (9)].

In Hartree-Fock theory, the LUMO represents an extra electron in the field of all the electrons (except itself) of the molecule. This corresponds to the electron affinity needed for Equation (9). However, in Kohn-Sham DFT (LDA; GGA, meta-GGA DFs), the LUMO represents an electron excited from a lower occupied orbital instead of an added electron.[124] This is due to the correction for the self-interaction error. Therefore, the LUMO energies do not correspond to the electron affinity, and Equation (9) cannot be applied. The LUMO energies in hybrid DFs lies between pure Kohn-Sham DFT and Hartree-Fock. Assary and coworker[23] also used LUMO energies calculated with a hybrid DF to estimate the reduction potentials, even though the LUMO does not correspond to the electron affinity. We tested the same procedure and evaluated the results. Figure 6 shows the oxidation and reduction potentials calculated from the HOMO and LUMO energies of the radical and reduced species. The deviations are depicted in Figure S11.

Only two DFs show a good agreement with the experimental potentials. In both cases, the oxidation and reduction potentials are calculated from the HOMO energy, while the reduction potentials estimated from the LUMO showed poor agreement with the experimental value. Furthermore, both DFs are hybrid functionals. GGA and meta-GGA DFs generally show poor agreement when the HOMO energy is used. The hybrid GGA B3LYP-D3(BJ) displays the best agreement with the experimental potentials ($\Delta_{Ox-HOMO} = -0.08$ V, $\Delta_{Red-LUMO} = 0.85$ V, $\Delta_{Red-HOMO} = 0.01$ V), and CCSD(T)/cbs (Q→aV5Z)* ($\Delta^{CCSD(T)}_{Ox-HOMO} = -0.02$ V, $\Delta^{CCSD(T)}_{Red-LUMO} = 0.88$ V, $\Delta^{CCSD(T)}_{Red-HOMO} = 0.04$ V). MN12-SX has the second-best agreement ($\Delta_{Ox-HOMO} = 0.08$ V, $\Delta_{Red-LUMO} = 0.48$ V, $\Delta_{Red-HOMO} = 0.03$ V, $\Delta^{CCSD(T)}_{Ox-HOMO} = 0.14$ V, $\Delta^{CCSD(T)}_{Red-LUMO} = 0.52$ V, $\Delta^{CCSD(T)}_{Red-HOMO} = 0.06$ V). It is a screened hybrid meta-GGA functional, which means that the Hartree-Fock exchange goes to 0% in the long-range part of the DF. The larger the amount of exact Hartree-Fock exchange, the more the physical meaning of the LUMO energy corresponds to the electron affinity. Therefore, we expected that a larger exact Hartree-Fock exchange would improve agreement for the reduction potential calculated from the LUMO energy. In particular, the DFs that differ only in the amount of Hartree-Fock exchange (such as B3LYP and BHYLP, PBE and PBE0, TPSS and TPSSh) show the opposite. Increasing the exact Hartree-Fock exchange decreases the agreement between reduction potential calculated from the LUMO energy and the experiment

values as well as the CCSD(T)/cbs(Q→aV5Z)* results. The DFs with the best agreement to the experimental and CCSD(T)/CCSD(T)/cbs (Q→aV5Z)* reduction potential, when calculated from the LUMO energy GGA and meta-GGA functionals, are BP86-D3(BJ) ($\Delta_{Ox-HOMO} = 0.32\,V$, $\Delta_{Red-LUMO} = 0.04\,V$, $\Delta_{Red-HOMO} = 0.39\,V$, $\Delta^{CCSD(T)}_{Ox-HOMO} = 0.38\,V$, $\Delta^{CCSD(T)}_{Red-LUMO} = 0.07\,V$, $\Delta^{CCSD(T)}_{Red-HOMO} = 0.42\,V$) and the second best agreement is exhibit by using M11-L ($\Delta_{Ox-HOMO} = 0.31\,V$, $\Delta_{Red-LUMO} = 0.06\,V$, $\Delta_{Red-HOMO} = 0.19\,V$, $\Delta^{CCSD(T)}_{Ox-HOMO} = 0.37\,V$, $\Delta^{CCSD(T)}_{Red-LUMO} = 0.09\,V$, $\Delta^{CCSD(T)}_{Red-HOMO} = 0.22\,V$). Coincidentally, these two functionals also give the best agreement when the Gibbs energy is used to calculate the oxidation and reduction potentials.

3.2 | Developing the multistep screening procedure

In this section, a multistep screening procedure for the **1-X-R**-type molecules is developed and presented. The aim is to find molecules that have either a very low oxidation potential or a high reduction potential. The multistep screening procedure consists of three steps. In the first step, the oxidation and reduction potential are calculated for all possible molecules with a fast but less accurate method. The next two steps will each increase the accuracy, but also the computational effort. Only the best candidates are used for the next step.

The different methods employed have only limited accuracy. Therefore, it is not possible to simply select the molecule with the lowest oxidation or highest reduction potential at a given step. Instead, all molecules within an estimated error range of the method have to be considered. In the next section, we will select the methods and define the error range, that we also refer to as the selection cut-off. We use the experimental oxidation potentials of **1-O-Me**, **1-O-Bn**, **1-S-Me**, and **1-NH-Me** and the experimental reduction potentials of **1-O-Me**, **1-O-Bn**, and **1-S-Me**, for comparison.[27] The reduction potential **1-NH-Me** is not taking into account because of dimer formation.[27]

3.2.1 | First step: Crest and xTB

In the first step, a conformer search is performed with the Crest program package. Finally, Crest is used to calculate the total energies of the molecules with the semi-empirical method GFN2-xTB. The results can also be used to calculate the oxidation and reduction potentials. We showed in Figure 5 that GFN2-xTB with the solvent model ALPB and GBSA strongly overestimate the oxidation potential and reduction for **1-O-Me** by about 3.9 and 2.5 V, respectively. However, the **1-X-R**-type molecules have 7 different positions that can be differently substituted, X, R, and the 4 hydrogens in the benzo[*d*]-X-zolyl group (see Figure 10). This leads to tens of thousands of different candidate molecules. The xTB method allow these to be calculated in a reasonable time frame, being several orders of magnitude faster than DFT and wave function-based methods. Furthermore, GFN2-xTB (ALPB) and GFN2-xTB (GBSA) are much better at predicting the differences between the molecules, which is our focus. Figure 7A displays the oxidation potentials for **1-O-Me**, **1-O-Bn**, **1-S-Me**, and **1-NH-Me,** and Figure 7B the reduction potentials for **1-O-Me**, **1-O-Bn**, and **1-S-Me**. The calculated potentials have been shifted by a fixed value to improve the visibility of the trend. The unshifted data are shown in Figures S10 and S11. For GFN2-xTB (ALPB) and GFN2-xTB (GBSA) the oxidation potentials are shifted by −4.89 and −4.91 V, respectively. The reduction potentials are shifted by −4.29 and by −4.38 V, respectively. Figures 7, S12 and S13 show the calculated results (abscissa) plotted against the experimental results (ordinate). When the calculated and experimental values are the same, they lie on the black dashed line.

The ALPB and GBSA solvent models gave similar results, with GFN2-xTB (ALPB) showing a 0.005 V smaller deviation from the experimental trend for the oxidation potential. For both solvent models, GFN2-xTB incorrectly predicts the order of the **1-X-R**-type molecules for the oxidation potentials. GFN2-xTB (ALPB) incorrectly predicts **1-S-Me** to have a higher oxidation potential than **1-O-Me**. GFN2-xTB (GBSA) even predicts **1-S-Me** to have a higher oxidation potential than **1-O-Me** and also **1-O-Bn**. The order of the **1-X-R**-type molecules for the reduction potentials is predicted correctly by both approaches, but the deviations are of a similar magnitude as for the oxidation potentials.

Since GFN2-xTB (ALPB) predicts the order of the **1-X-R**-type molecules for the oxidation potentials better than GFN2-xTB (GSBA), we use GFN2-xTB (ALPB) in the screening approach. For the accuracy of the method, we use the largest error we found for predicting the difference between two **1-X-R**-type molecules. In case of GFN2-xTB (ALPB) this is the difference between the oxidation potential of **1-S-Me** (overestimated by 0.07 V) and **1-NH-Me** (underestimated by 0.09 V). The experimental difference Δ_{Exp} between them is 0.18 V, the calculated difference Δ_{Calc} is 0.32 V (see the yellow and orange arrow in Figure 7). Thus, we estimate that GFN2-xTB (ALPB) has an error of up to 0.16 V ($|\Delta_{Exp} - \Delta_{Calc}|$). Since the data set is small, we estimate the error range for our screening approach to be twice as large, that is, 0.32 V. This means that in the first step of the screening approach, a conformer search is performed with Crest for all molecules and their oxidation and reduction potentials are calculated with GFN2-xTB (ALPB). The molecule with the lowest oxidation potential and all molecules up to 0.32 V above, and the molecule with the highest reduction potential and all molecules 0.32 V below are selected for the second screening step. This is also illustrated in Figure 10.

3.2.2 | Second step: Orbital energies

In the second step, the oxidation and reduction potentials are estimated from the orbital energies of the **1-X-R** type molecules. We showed and discussed that predictions based on the HOMO energy are more accurate and physically more meaningful. Therefore, we use the HOMO energies of the radical species $E^{Radical}_{HOMO}$ and reduced spices E^{Anion}_{HOMO} to estimate the oxidation and reduction potentials,

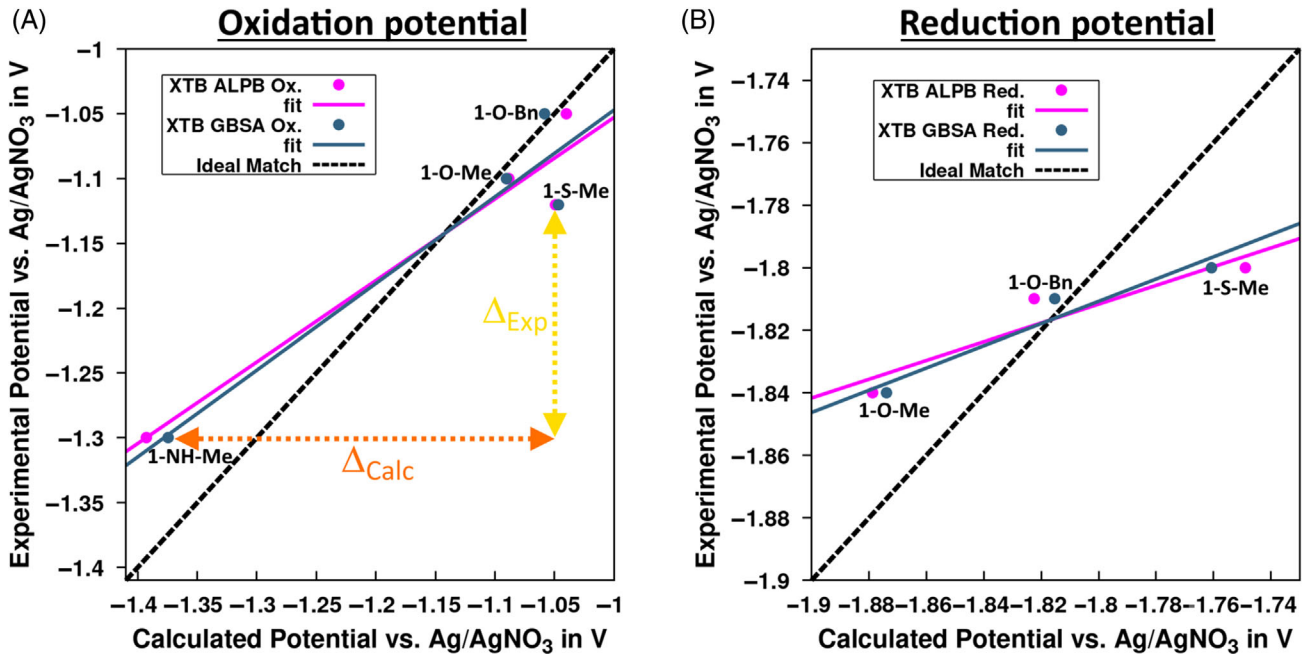

FIGURE 7 (A) E_{Ox} of **1-O-Me**, **1-O-Bn**, **1-S-Me**, and **1-NH-Me**, (B) E_{Red} of **1-O-Me**, **1-O-Bn**, and **1-S-Me**. The calculations are performed at xTB level of theory. For GFN2-xTB (ALPB) and GFN2-xTB (GBSA) the oxidation potentials are shifted by −4.89 and −4.91 V, respectively. The reduction potentials are shifted by −4.29 and by −4.38 V, respectively. The unshifted data are presented in Figures S10 and S11. The calculated value is the abscissa, and the experimental value is the ordinate of the data points. When the calculated and experimental value are equal, they lie on the black dashed line. The pink and green lines (fit) are the lines of best fit through the GFN2-xTB (ALPB) and GFN2-xTB (GBSA) data points, respectively. Δ_{Exp} and the corresponding yellow arrow is the experimental difference between the oxidation potentials of **1-S-Me**, and **1-NH-Me**. Δ_{Calc} and the corresponding orange arrow is the calculated difference between these reduction potentials.

respectively. The DF B3LYP-D3(BJ) has the best agreement with the experimental results (Figure 6). To reduce the computational time, the split-valence basis set def2-SVP is used instead of the more demanding triple-ζ def2-TZVP basis set. In addition, we also employed the DF PBE0-D3(BJ), because it is nonempirical.

We modified the Hartree-Fock exchange of both to improve the agreement of the oxidation and reduction potentials for the molecules **1-O-Me**, **1-O-Bn**, **1-S-Me**, and **1-NH-Me** as described in the computational details (also see Figures S14–S21). Modifying the Hartree-Fock exchange of B3LYP and PBE0 is a common practice.[73,99,100,125] For example, Reiher et al.[99] reparametrized B3LYP in this way to better describe the low-spin/high-spin energy splitting for Fe(II) complexes. Atalla et al.[125] reparametrized PBE0 so that its LUMO energy represents the electron affinity. For the presented calculation of the oxidation potential the Hartree-Fock exchange of B3LYP-D3(BJ)/def2-SVP and PBE0-D3(BJ)/def2-SVP were changed to 20.49% and 16.05%, respectively. To identify them, the functionals are referred to herein as B3LYP-D3(BJ)$^+$ and PBE0-D3(BJ)$^+$. For the calculation of the reduction potential, the Hartree-Fock exchange of B3LYP-D3(BJ)/def2-SVP and PBE0-D3(BJ)/def2-SVP were changed to 28.04% and 24.83%, respectively. To identify them, the modified DF referred to here as B3LYP-D3(BJ)$^-$ and PBE0-D3(BJ)$^-$.

Figure 8 displays the results. For the accuracy of the method, we again use the largest error we found for predicting the difference between two **1-X-R** type molecules. The errors for the oxidation potentials are about twice as large as those for reduction potentials. The largest error of all is the difference between the oxidation potential of **1-S-Me** [which is overestimated by 0.03 V with B3LYP-D3(BJ)$^+$ and by 0.04 V with PBE0-D3(BJ)$^+$] and **1-NH-Me** [which is underestimated by 0.03 V with B3LYP-D3(BJ)$^+$ and by 0.04 V with PBE0-D3(BJ)$^+$]. Accordingly, the trend between them is off by 0.06 V for B3LYP-D3(BJ)$^+$ and 0.08 V for PBE0-D3(BJ)$^+$. Since B3LYP-D3(BJ)$^+$ has the smaller deviation, we use the B3LYP-D3(BJ) DF for the screening. For the screening approach, we again estimate that the selection cut-off to be twice as large as the largest deviation found, that is, 0.12 V. Thus, the molecules with the best oxidation and reduction potential and all molecules within 0.12 V will be selected for the final step (see also Figure 10).

3.2.3 | Third step: Gibbs energies

In the last step, the oxidation and reduction potentials are calculated based on the Gibbs energies of the redox reactions [Equations (5) and (6)]. As shown, M11-L/def2-TZVP and BP86-D3(BJ)/def2-TZVP show the best agreement with the experimental redox potentials and the theoretical benchmark values. In contrast to the DFT-D3(BJ) approach, the M11-L DF has been overserved to not properly describe London dispersion.[126] Since our experimental investigation

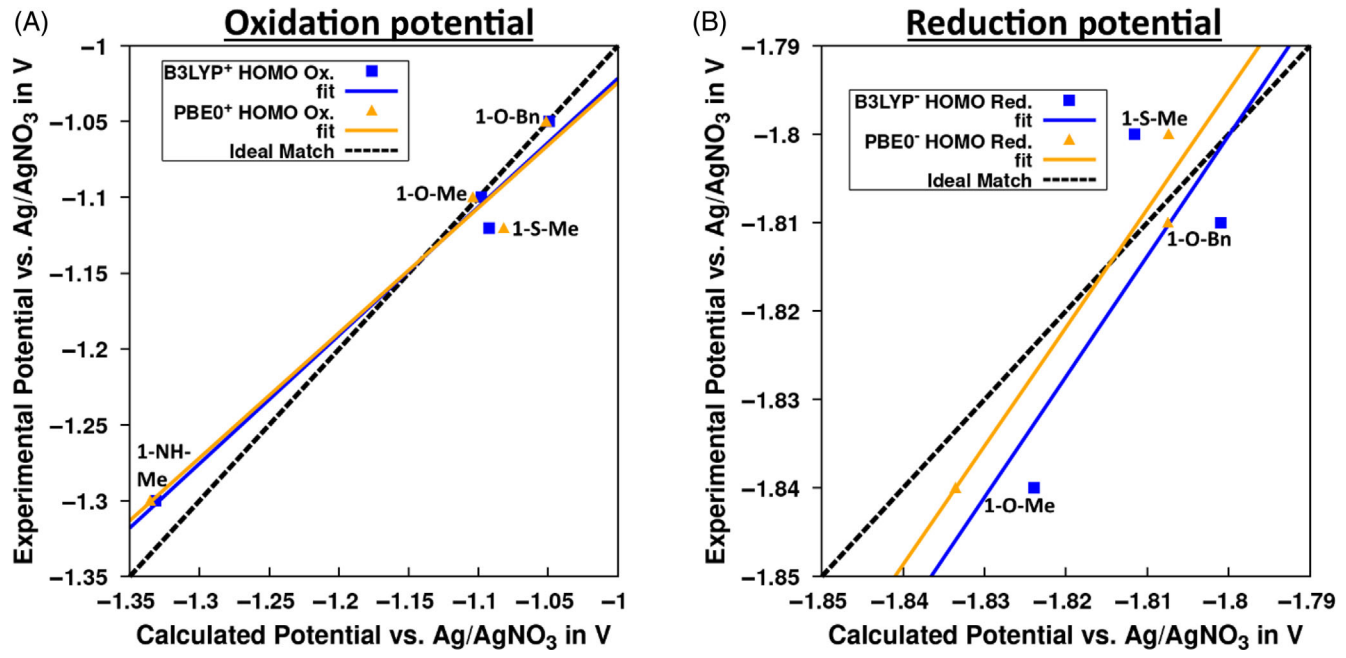

FIGURE 8 (A) E_{Ox} of **1-O-Me**, **1-O-Bn**, **1-S-Me**, and **1-NH-Me**, (B) E_{Red} of **1-O-Me**, **1-O-Bn**, and **1-S-Me**. The calculated value is the abscissa, and the experimental value is the ordinate of the data points. When the calculated and experimental values are the same, they will lie on the black dashed line. The HOMO energy is used to calculate the oxidation and reduction potentials. Calculations are performed (A) with B3LYP-D3(BJ)$^{+}$/def2-SVP (blue squares) and PBE0-D3(BJ)$^{+}$/def2-SVP (orange triangles) levels of theory, and (B) B3LYP-D3(BJ)$^{-}$/def2-SVP (blue squares) and PBE0-D3(BJ)$^{-}$/def2-SVP (orange triangles) levels of theory. Trend linens are added to visualize the trends.

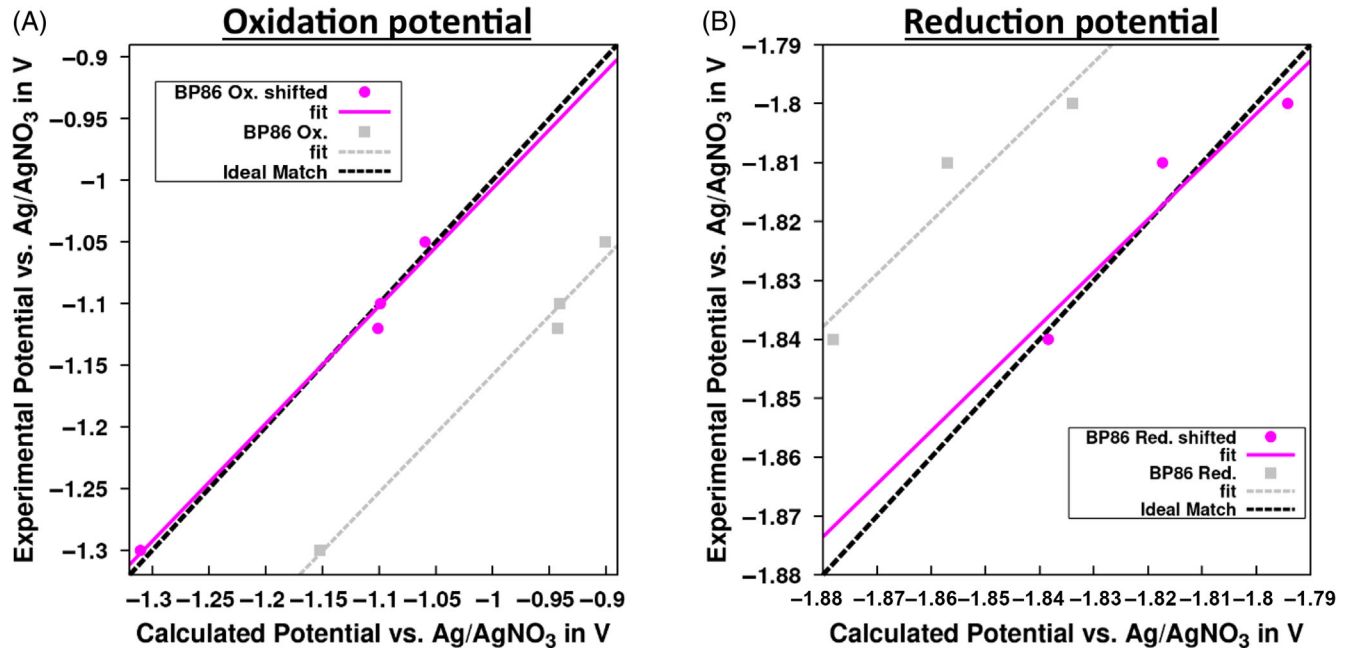

FIGURE 9 (A) E_{Ox} of **1-O-Me**, **1-O-Bn**, **1-S-Me**, and **1-NH-Me**, (B) E_{Red} of **1-O-Me**, **1-O-Bn**, and **1-S-Me**. The calculations are performed with BP86-D3(BJ)/def2-TZVP (DCOSMO-RS-out). For better visibility, the calculated oxidation and reduction potentials have been shifted by −0.159 and +0.040 V, respectively. The calculate value is the abscissa, and the experimental value is the ordinate of the pink data points. If calculated and experimental value are the same, they will be on the black dashed line. The data points with unshifted calculated values on the abscissa are shown in gray. The pink line (fit) and the gray dashed line (fit) are the lines of best fit through the corresponding data points.

indicates the formation of van der Waals bound dimers for 1-NH-Me and its derivatives,[27] we decided to use BP86-D3(BJ)/def2-TZVP. The solvent effects are included with DCOSMO-RS-out.

The results are shown in Figure 9 in gray. The calculated oxidation and reduction potentials are plotted against the experimental ones. As shown, BP86-D3(BJ)/def2-TZVP (DCOSMO-RS-out)

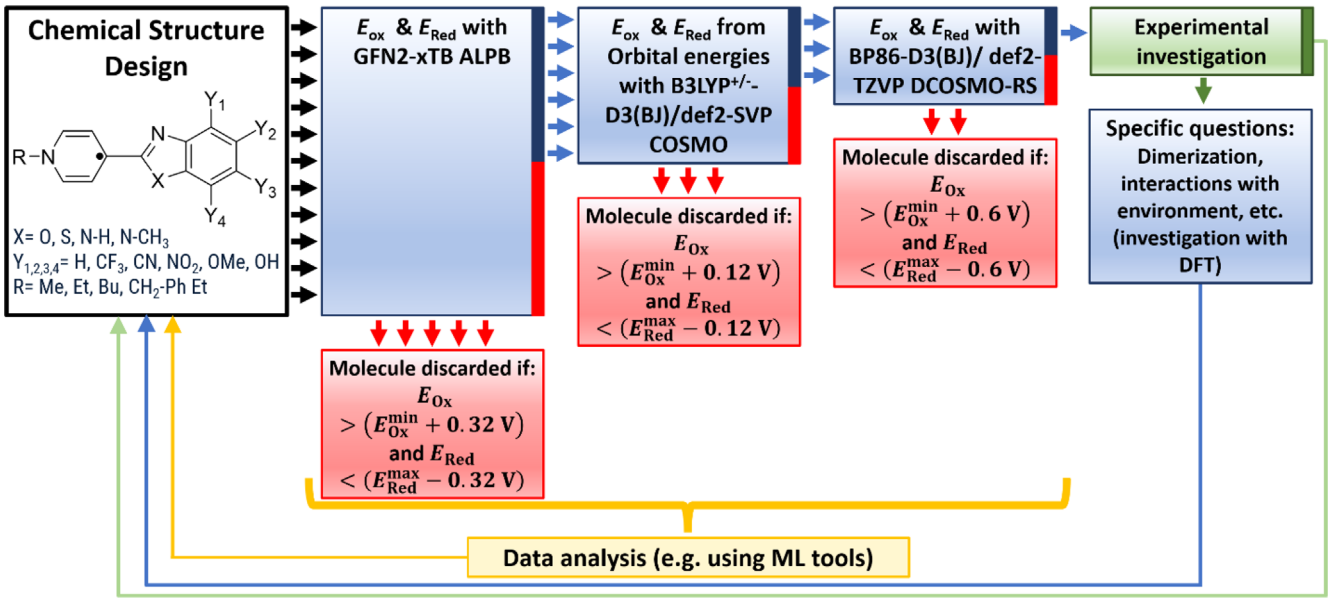

FIGURE 10 Schematic depiction of the multistep screening procedure from left to right, with the method for each step explained. In the three screening steps, the oxidation and reduction potentials of the candidate molecules are calculated. The molecules that fit the selection criteria are moved to the next step. The red boxes give the criteria for a molecule to not be considered for the next step: The calculated oxidation potential E_{Ox} is larger than the lowest calculated oxidation potential E_{Ox}^{min} added with the estimated error range, and the molecule has also a calculated reduction potential E_{Red} that is smaller than the highest calculated reduction potential E_{Red}^{max} subtracted by the estimated error range.

slightly overestimates the oxidation potential, and slightly underestimates the reduction potential. However, the deviation from the experimental trend of the oxidation and reduction potentials is even smaller. We shifted the oxidation potentials by −0.159 V and the reduction potentials by +0.040 V for better visualization. The shifted values are displayed in pink and the unshifted in gray in Figure 9. In contrast to the first two steps of the screening, the correct order of the molecules is predicted for the oxidation and reduction potentials. The largest error is the difference between the oxidation potential of **1-S-Me** (overestimated by 0.02 V) and **1-NH-Me** (underestimated by 0.01 V). The trend between them is off by 0.03 V. Accordingly, we estimate the error range for this step of the screening approach to be 0.06 V as shown in Figure 10, this is independent of the shifts we used for the visualization. The entire screening procedure is explained below.

3.2.4 | The multistep screening procedure

Figure 10 shows the screening procedure for the **1-X-R**-type molecules. Initially, a large number of possible **1-X-R**-type molecules with different hetero atoms **X**, linkers **R**, and also substituent **Y** are generated. These molecules go through a three-step screening process. At each step, the molecule with lowest oxidation potential, and the molecules with the highest reduction potential are selected for the next step. In addition, all molecules whose oxidation or reduction potentials differs by less than the estimated error range of the method from the oxidation or reduction potential of the best candidate are also considered. In the first step a conformer search is performed with Crest. The oxidation or reduction potentials are calculated at the GFN2-xTB (ALPB) level of theory with an estimated error range of 0.32 V. In the second step, the oxidation and reduction potentials are estimated from the HOMO energies of the radical and reduced species. B3LYP-D3(BJ)$^{+}$/def2-SVP is used for the oxidation, and the B3LYP-D3(BJ)$^{-}$/def2-SVP for the reduction potential. For both, the error is here estimated to be 0.12 V. In the final step, the oxidation and reduction potentials are calculated from Gibbs energies of the redox reactions with BP86-D3(BJ)/def2-TZVP (DCOSMO-RS-out). The error here is estimated to be 0.06 V. The molecules selected in the last step are subsequently investigated experimentally and deeply theoretically. Additional questions that have already arisen (see Ref. 27) or will arise during the experimental investigation can also be investigated at, for example, BP86-D3(BJ)/def2-TZVP (DCOSMO-RS-out) level of theory. Possible investigations could be, for example, dimer formation, interaction with electrolyte, solvent, and the influence of the polymer chain. Stability or reactivity can also be assessed.

During the screening, the oxidation and reduction potentials of a large number of molecules are calculated. These can be used to gain insight into the structure–property-relationship of **1-X-R**-type molecules as we found in study[17] of substituted quinones. Machine learning tools could potentially be used to analyze these data. The results of the structure–property-relationships, the experimental investigation, and the investigation of the additional questions can also be used to create design principles and design a new set of possible molecules. This new set can then be again screened using the multistep screening procedure with possibly adjusted error ranges.

4 | CONCLUSIONS

Viologens have shown desirable properties for use in organic RFBs and PBBs.[8–13] **1-X-R**-type molecules (Scheme 1) represent improved viologens in which three different heteroatomic groups **X**, organic linker **R**, and functional groups at the benzo group can be introduced. Thus, thousands differently substituted **1-X-R**-type molecules are possible. To identify the most promising candidates, an in silico multistep screening procedure is developed in the presented study. Experimental data[27] are used as reference data throughout the study.

In the first part, wave function-based methods are used to determine additional reference data. Oxidation and reduction potentials calculated with CCSD(T)/cbs(Q→aV5Z)* in conjunction with the DCOSMO-RS solvent model with outlying charge correction are subsequently used together with corresponding experimental values as a reference for a method evaluation. Different methods (semi-empirical, DFT, wave function-based), solvent models, dispersion corrections, and basis sets for the calculation of oxidation and reduction potentials of **1-X-R**-type molecular derivatives are evaluated.

Solvent models revealed better agreement with experimental and CCSD(T)/cbs(Q→aV5Z)* reference from left to right: IEFPCM < SMD < COSMO ≈ COSMO-ion < DCSOMO-RS < COSMO-out ≈ COSMO-ion-out < DCOSMO-RS-out ≈ DCOSMO-RS-out-c. At the DFT level, the basis set limit was basically reached at the def2-QZVP level. Additional polarization or diffuse functions are not required. With def2-TZVP the DFT calculations underestimate the oxidation and reduction potentials by 0.02 and 0.04 V, respectively, compared to the DFT basis set limit. Dispersion corrections in conjunction with the B3LYP DF revealed better agreement with experiment along the order: VV10 < D3(BJ) < D4. D4 was the best, but it may have problems with frequency calculations. Therefore, we recommend D3(BJ) for screening purposes. Twenty-nine different DFs were evaluated, including all commonly used types. In addition, the Hartree-Fock-based HF-3c/minix approach was assessed. M11-L, SVWN, and BP86-D3(BJ) showed the best agreement with the reference data.

The HOMO and LUMO energies of the radical and reduced species calculated with 27 DFs were used to estimate the oxidation and reduction potentials. For the calculation of the reduction potential from the LUMO energy, the GGA and meta-GGA DFs, in particular M11-L and BP86-D3(BJ), show the best agreement with the reference data. The hybrid functionals B3LYP and MN12-SX give the best agreement with the experimental values, when the HOMO energies are used to estimate the oxidation and reduction potentials.

In the second part, we propose a multistep screening procedure of redox-active organic molecules for PBBs and RFBs. The molecules are selected according to their oxidation or reduction potential. With each step, the method becomes more accurate, but also more time consuming. In the first step, a conformer search is performed with Crest and the oxidation or reduction potentials are calculated with GFN2-xTB (ALPB). Second, the oxidation and reduction potential are estimated form the HOMO energies calculated with B3LYP-D3(BJ)$^{+}$/def2-SVP and B3LYP-D3(BJ)$^{-}$/def2-SVP. These are B3LYP DFs with optimized Hartree-Fock exchange. In the final step, the oxidation and reduction potential are calculated from the Gibbs energies of the redox reactions with BP86-D3(BJ)/def2-TZVP.

Next, we will apply our proposed multistep procedure to a large number of differently substituted **1-X-R**-type molecules to find suitable candidates. We also assume that this multiscreening procedure can be transferred to other organic redox active molecules and in particular aromatic molecules/radicals. Considering other redox active molecules, we recommend checking and adjusting the selection cutoffs estimated in this study for **1-X-R**-type molecules.

ACKNOWLEDGMENTS

This work was founded by the German Research Foundation (DFG) within priority program "Polymer-based Batteries" (SPP 2248, project number 441217366). We acknowledge computational resources provided by the HPC Core Facility and the HRZ of the Justus Liebig University Giessen. Open Access funding enabled and organized by Projekt DEAL.

DATA AVAILABILITY STATEMENT

The data that supports the findings of this study are available in the supplementary material of this article.

ORCID

Andreas J. Achazi https://orcid.org/0000-0002-3001-875X

Doreen Mollenhauer https://orcid.org/0000-0003-0084-4599

REFERENCES

[1] J. Winsberg, T. Hagemann, T. Janoschka, M. D. Hager, U. S. Schubert, *Angew. Chem. Int. Ed.* **2017**, *56*, 686.
[2] J. Winsberg, T. Hagemann, T. Janoschka, M. D. Hager, U. S. Schubert, *Am. Ethnol.* **2017**, *129*, 702.
[3] Y. Ding, C. Zhang, L. Zhang, Y. Zhou, G. Yu, *Chem. Soc. Rev.* **2018**, *47*, *69*.
[4] S. Muench, A. Wild, C. Friebe, B. Häupler, T. Janoschka, U. S. Schubert, *Chem. Rev.* **2016**, *116*, 9438.
[5] M. C. Krishna, D. A. Grahame, A. Samuni, J. B. Mitchell, A. Russo, *Proc. Natl. Acad. Sci.* **1992**, *89*, 5537.
[6] M. D. Hager, B. Esser, X. Feng, W. Schuhmann, P. Theato, U. S. Schubert, *Adv. Mater.* **2020**, *32*, 2000587.
[7] A. Zaichenko, A. J. Achazi, S. Kunz, H. A. Wegner, J. Janek, D. Mollenhauer, *Prog. Ener.* **2024**, *6*, 12001.
[8] X.-L. Lv, P. Sullivan, H.-C. Fu, X. Hu, H. Liu, S. Jin, W. Li, D. Feng, *ACS Energy Lett.* **2022**, *7*, 2428.
[9] C. Chen, S. Zhang, Y. Zhu, Y. Qian, Z. Niu, J. Ye, Y. Zhao, X. Zhang, *RSC Adv.* **2018**, *8*, 18762.
[10] M. Yao, H. Sano, H. Ando, T. Kiyobayashi, *Sci. Rep.* **2015**, *5*, 1.
[11] S. Sen, J. Saraidaridis, S. Y. Kim, G. T. R. Palmore, *ACS Appl. Mater. Interfaces* **2013**, *5*, 7825.
[12] N. Sano, W. Tomita, S. Hara, C.-M. Min, J.-S. Lee, K. Oyaizu, H. Nishide, *ACS Appl. Mater. Interfaces* **2013**, *5*, 1355.
[13] K. Koshika, N. Chikushi, N. Sano, K. Oyaizu, H. Nishide, *Green Chem.* **2010**, *12*, 1573.
[14] P. Savarino, G. Viscardi, P. Quagliotto, P. Perracino, E. Barni, *J. Heterocyclic Chem.* **1997**, *34*, 1479.
[15] J. D. Hofmann, S. Schmalisch, S. Schwan, L. Hong, H. A. Wegner, D. Mollenhauer, J. R. Janek, D. Schröder, *Chem. Mater.* **2020**, *32*, 3427.
[16] S. Kunz, M. J. van Rensburg, D. S. Pietruschka, A. J. Achazi, D. Emmel, D. Mollenhauer, H. A. Wegner, D. Schröder, *Chem. Mater.* **2022, 34, 10424**. https://doi.org/10.1021/acs.chemmater.2c02279

[17] S. Schwan, D. Schröder, H. Wegner, J. Janek, D. Mollenhauer, *ChemSusChem* **2020**, *13*, 5480.
[18] R. P. Fornari, P. de Silva, *Wiley Interdiscip. Rev.: Comput. Mol. Sci.* **2021**, *11*, e1495.
[19] S. Er, C. Suh, M. P. Marshak, A. Aspuru-Guzik, *Chem. Sci.* **2015**, *6*, 885.
[20] L. Cheng, R. S. Assary, X. Qu, A. Jain, S. P. Ong, N. N. Rajput, K. Persson, L. A. Curtiss, *J. Phys. Chem. Lett.* **2015**, *6*, 283.
[21] D. P. Tabor, R. Gómez-Bombarelli, L. Tong, R. G. Gordon, M. J. Aziz, A. Aspuru-Guzik, *J. Mater. Chem. A* **2019**, *7*, 12833.
[22] C.-H. Li, D. P. Tabor, *J. Mater. Chem. A* **2022**, *10*, 8273.
[23] J. E. Bachman, L. A. Curtiss, R. S. Assary, *J. Phys. Chem. A* **2014**, *118*, 8852.
[24] Q. Zhang, A. Khetan, S. Er, *Sci. Rep.* **2020**, *10*, 1.
[25] R. Duke, V. Bhat, P. Sornberger, S. A. Odom, C. Risko, *Digit. Discov.* **2023**, *2*, 1152.
[26] J. Ho, M. L. Coote, C. J. Cramer, D. G. Truhlar, in *Organic Electrochemistry* (Eds: O. Hammerich, B. Speiser), CRC Press, Boca Raton, FL **2016**, p. 229.
[27] X. Fataj, A. J. Achazi, P. Rohland, E. Schröter, S. Muench, R. Burges, K. L. H. Pohl, D. Mollenhauer, M. D. Hager, U. S. Schubert, *Chem. Eur. J.* **2023, e202302979**.
[28] W. Zhang, T. Yang, K. Zhao, X. Liao, Y. Zhao, *Int. J. Quantum Chem.* **2022**, *122*, e26886.
[29] P. Pracht, F. Bohle, S. Grimme, *Phys. Chem. Chem. Phys.* **2020**, *22*, 7169.
[30] P. Pracht, S. Grimme, *Chem. Sci.* **2021**, *12*, 6551.
[31] S. Grimme, *J. Chem. Theory Comput.* **2019**, *15*, 2847.
[32] C. Bannwarth, S. Ehlert, S. Grimme, *J. Chem. Theory Comput.* **2019**, *15*, 1652.
[33] S. Grimme, C. Bannwarth, P. Shushkov, *J. Chem. Theory Comput.* **2017**, *13*, 1989.
[34] P. Pracht, E. Caldeweyher, S. Ehlert, S. Grimme, *ChemRxiv* **2019**, 1. https://chemrxiv.org/engage/chemrxiv/article-details/60c742abbdbb890c7ba3851a
[35] S. Ehlert, M. Stahn, S. Spicher, S. Grimme, *J. Chem. Theory Comput.* **2021**, *17*, 4250.
[36] TURBOMOLE V751 2021, A development of University of Karlsruhe and Forschungszentrum Karlsruhe Gmbh, 1989–2007, TURBOMOLE GmbH. **2007** Available from http://www.turbomole.com
[37] R. Ahlrichs, M. Bär, M. Häser, H. Horn, C. Kölmel, *Chem. Phys. Lett.* **1989**, *162*, 165.
[38] S. G. Balasubramani, G. P. Chen, S. Coriani, M. Diedenhofen, M. S. Frank, Y. J. Franzke, F. Furche, R. Grotjahn, M. E. Harding, C. Hättig, A. Hellweg, B. Helmich-Paris, C. Holzer, U. Huniar, M. Kaupp, A. M. Khah, S. K. Khani, T. Müller, F. Mack, B. D. Nguyen, S. M. Parker, E. Perlt, D. Rappoport, K. Reiter, S. Roy, M. Rückert, G. Schmitz, M. Sierka, E. Tapavicza, D. P. Tew, C.v. Wüllen, V. K. Voora, F. Weigend, A. Wodyński, J. M. Yu, *J. Chem. Phys.* **2020**, *152*, 184107.
[39] M. J. Frisch, G. W. Trucks, H. B. Schlegel, G. E. Scuseria, M. A. Robb, J. R. Cheeseman, G. Scalmani, V. Barone, G. A. Petersson, H. Nakatsuji, X. Li, M. Caricato, A. V. Marenich, J. Bloino, B. G. Janesko, R. Gomperts, B. Mennucci, H. P. Hratchian, J. V. Ortiz, A. F. Izmaylov, J. L. Sonnenberg, Williams, F. Ding, F. Lipparini, F. Egidi, J. Goings, B. Peng, A. Petrone, T. Henderson, D. Ranasinghe, V. G. Zakrzewski, J. Gao, N. Rega, G. Zheng, W. Liang, M. Hada, M. Ehara, K. Toyota, R. Fukuda, J. Hasegawa, M. Ishida, T. Nakajima, Y. Honda, O. Kitao, H. Nakai, T. Vreven, K. Throssell, J. A. Montgomery Jr., J. E. Peralta, F. Ogliaro, M. J. Bearpark, J. J. Heyd, E. N. Brothers, K. N. Kudin, V. N. Staroverov, T. A. Keith, R. Kobayashi, J. Normand, K. Raghavachari, A. P. Rendell, J. C. Burant, S. S. Iyengar, J. Tomasi, M. Cossi, J. M. Millam, M. Klene, C. Adamo, R. Cammi, J. W. Ochterski, R. L. Martin, K. Morokuma, O. Farkas, J. B. Foresman, D. J. Fox, Gaussian 09, Revision B.01. Gaussian Inc. Wallingford, CT **2016**.
[40] P. A. M. Dirac, Proceedings of the Royal Society of London Series A, Containing Papers of a Mathematical and Physical Character. **1929** 123 (792), 714–733.
[41] J. C. Slater, *Phys. Rev.* **1951**, *81*, 385.
[42] S. H. Vosko, L. Wilk, M. Nusair, *Can. J. Phys.* **1980**, *58*, 1200.
[43] A. D. Becke, *Phys. Rev. A* **1988**, *38*, 3098.
[44] C. Lee, W. Yang, R. G. Parr, *Phys. Rev. B* **1988**, *37*, 785.
[45] A. D. Becke, *J. Chem. Phys.* **1993**, *98*, 5648.
[46] S. Grimme, J. Antony, S. Ehrlich, H. Krieg, *J. Chem. Phys.* **2010**, *132*, 154104.
[47] S. Grimme, S. Ehrlich, L. Goerigk, *J. Comput. Chem.* **2011**, *32*, 1456.
[48] F. Weigend, R. Ahlrichs, *Phys. Chem. Chem. Phys.* **2005**, *7*, 3297.
[49] F. Weigend, *Phys. Chem. Chem. Phys.* **2006**, *8*, 1057.
[50] S. F. Sousa, P. A. Fernandes, M. J. Ramos, *J. Phys. Chem. A* **2007**, *111*, 10439.
[51] S. Grimme, M. Steinmetz, *Phys. Chem. Chem. Phys.* **2013**, *15*, 16031.
[52] K. Eichkorn, O. Treutler, H. Öhm, M. Häser, R. Ahlrichs, *Chem. Phys. Lett.* **1995**, *240*, 283.
[53] K. Eichkorn, O. Treutler, H. Oehm, M. Häser, R. Ahlrichs, *Chem. Phys.* **1995**, *242*, 652.
[54] K. Eichkorn, F. Weigend, O. Treutler, R. Ahlrichs, *Theor. Chem. Acc.* **1997**, *97*, 119.
[55] A. Schäfer, A. Klamt, D. Sattel, J. C. Lohrenz, F. Eckert, *Phys. Chem. Chem. Phys.* **2000**, *2*, 2187.
[56] A. Klamt, G. Schüürmann, *J. Chem. Soc., Perkin Trans.* **1993**, *2*, 799.
[57] I. M. Smallwood, *Handbook of Organic Solvent Properties*, Hodder Headline Group, London, United Kingdom **1996**.
[58] D. R. Lide, W. M. Haynes, *CRC Handbook of Chemistry and Physics*, CRC press, Boca Raton, FL **2010**.
[59] P. Deglmann, F. Furche, *J. Chem. Phys.* **2002**, *117*, 9535.
[60] P. Deglmann, F. Furche, R. Ahlrichs, *Chem. Phys. Lett.* **2002**, *362*, 511.
[61] E. Caldeweyher, C. Bannwarth, S. Grimme, *J. Chem. Phys.* **2017**, *147*, 34112.
[62] E. Caldeweyher, S. Ehlert, A. Hansen, H. Neugebauer, S. Spicher, C. Bannwarth, S. Grimme, *J. Chem. Phys.* **2019**, *150*, 154122.
[63] O. A. Vydrov, T. Van Voorhis, *J. Chem. Phys.* **2010**, *133*, 244103.
[64] W. Hujo, S. Grimme, *Phys. Chem. Chem. Phys.* **2011**, *13*, 13942.
[65] F. Weigend, F. Furche, R. Ahlrichs, *J. Chem. Phys.* **2003**, *119*, 12753.
[66] D. Rappoport, F. Furche, *J. Chem. Phys.* **2010**, *133*, 134105.
[67] A. Klamt, V. Jonas, *J. Chem. Phys.* **1996**, *105*, 9972.
[68] A. Klamt, C. Moya, J. Palomar, *J. Chem. Theory Comput.* **2015**, *11*, 4220.
[69] J. Tomasi, B. Mennucci, R. Cammi, *Chem. Rev.* **2005**, *105*, 2999.
[70] J. Tomasi, B. Mennucci, E. Cancès, *J. Mol. Struct.: THEOCHEM* **1999**, *464*, 211.
[71] S. Sinnecker, A. Rajendran, A. Klamt, M. Diedenhofen, F. Neese, *J. Phys. Chem. A* **2006**, *110*, 2235.
[72] A. V. Marenich, C. J. Cramer, D. G. Truhlar, *J. Phys. Chem. B* **2009**, *113*, 6378.
[73] A. D. Becke, *J. Chem. Phys.* **1993**, *98*, 1372.
[74] T. Yanai, D. P. Tew, N. C. Handy, *Chem. Phys. Lett.* **2004**, *393*, 51.
[75] S. Grimme, *J. Chem. Phys.* **2006**, *124*, 34108.
[76] J. P. Perdew, *Phys. Rev. B* **1986**, *33*, 8822.
[77] J. P. Perdew, Y. Wang, *Phys. Rev. B* **1992**, *45*, 13244.
[78] J. P. Perdew, K. Burke, M. Ernzerhof, *Phys. Rev. Lett.* **1996**, *77*, 3865.
[79] J. P. Perdew, M. Ernzerhof, K. Burke, *J. Chem. Phys.* **1996**, *105*, 9982.
[80] J. Tao, J. P. Perdew, V. N. Staroverov, G. E. Scuseria, *Phys. Rev. Lett.* **2003**, *91*, 146401.
[81] V. N. Staroverov, G. E. Scuseria, J. Tao, J. P. Perdew, *J. Chem. Phys.* **2003**, *119*, 12129.

[82] Y. Zhao, D. G. Truhlar, *J. Phys. Chem. A* **2005**, *109*, 5656.
[83] Y. Zhao, D. G. Truhlar, *Theor. Chem. Acc.* **2008**, *120*, 215.
[84] Y. Zhao, D. G. Truhlar, *J. Chem. Theory Comput.* **2008**, *4*, 1849.
[85] R. Peverati, D. G. Truhlar, *J. Phys. Chem. Lett.* **2012**, *3*, 117.
[86] R. Peverati, D. G. Truhlar, *J. Phys. Chem. Lett.* **2011**, *2*, 2810.
[87] P. Verma, Y. Wang, S. Ghosh, X. He, D. G. Truhlar, *J. Phys. Chem. A* **2019**, *123*, 2966.
[88] R. Peverati, D. G. Truhlar, *Phys. Chem. Chem. Phys.* **2012**, *14*, 13171.
[89] R. Peverati, D. G. Truhlar, *Phys. Chem. Chem. Phys.* **2012**, *14*, 16187.
[90] H. S. Yu, X. He, D. G. Truhlar, *J. Chem. Theory Comput.* **2016**, *12*, 1280.
[91] H. S. Yu, X. He, S. L. Li, D. G. Truhlar, *Chem. Sci.* **2016**, *7*, 5032.
[92] J. W. Furness, A. D. Kaplan, J. Ning, J. P. Perdew, J. Sun, *J. Phys. Chem. Lett.* **2020**, *11*, 8208.
[93] J. Sun, A. Ruzsinszky, J. P. Perdew, *Phys. Rev. Lett.* **2015**, *115*, 36402.
[94] K. Hui, J.-D. Chai, *J. Chem. Phys.* **2016**, *144*, 44114.
[95] J.-D. Chai, M. Head-Gordon, *J. Chem. Phys.* **2008**, *128*, 84106.
[96] J.-D. Chai, M. Head-Gordon, *Phys. Chem. Chem. Phys.* **2008**, *10*, 6615.
[97] S. Grimme, J. G. Brandenburg, C. Bannwarth, A. Hansen, *J. Chem. Phys.* **2015**, *143*, 54107.
[98] S. Grimme, A. Hansen, S. Ehlert, J.-M. Mewes, *ChemRxiv* **2020**, 1. https://chemrxiv.org/engage/chemrxiv/article-details/60c75338702a9b696218c304
[99] M. Reiher, O. Salomon, B. A. Hess, *Theor. Chem. Acc.* **2001**, *107*, 48.
[100] A. Slimani, X. Yu, A. Muraoka, K. Boukheddaden, K. Yamashita, *J. Phys. Chem. A* **2014**, *118*, 9005.
[101] R. Sure, S. Grimme, *J. Comput. Chem.* **2013**, *34*, 1672.
[102] C. Møller, M. S. Plesset, *Phys. Rev.* **1934**, *46*, 618.
[103] R. A. Bachorz, F. A. Bischoff, A. Glöß, C. Hättig, S. Höfener, W. Klopper, D. P. Tew, *J. Comput. Chem.* **2011**, *32*, 2492.
[104] C. Hättig, D. P. Tew, A. Köhn, *J. Chem. Phys.* **2010**, *132*, 231102.
[105] S. Grimme, *J. Chem. Phys.* **2003**, *118*, 9095.
[106] Y. Jung, R. C. Lochan, A. D. Dutoi, M. Head-Gordon, *J. Chem. Phys.* **2004**, *121*, 9793.
[107] T. Helgaker, W. Klopper, H. Koch, J. Noga, *J. Chem. Phys.* **1997**, *106*, 9639.
[108] M. S. Marshall, L. A. Burns, C. D. Sherrill, *J. Chem. Phys.* **2011**, *135*, 194102.
[109] V. V. Pavlishchuk, A. W. Addison, *Inorg. Chim. Acta* **2000**, *298*, 97.
[110] W. A. Donald, M. Demireva, R. D. Leib, M. J. Aiken, E. R. Williams, *J. Am. Chem. Soc.* **2010**, *132*, 4633.
[111] W. A. Donald, R. D. Leib, J. T. O'Brien, M. F. Bush, E. R. Williams, *J. Am. Chem. Soc.* **2008**, *130*, 3371.
[112] W. A. Donald, R. D. Leib, M. Demireva, J. T. O'Brien, J. S. Prell, E. R. Williams, *J. Am. Chem. Soc.* **2009**, *131*, 13328.
[113] W. A. Donald, R. D. Leib, J. T. O'Brien, E. R. Williams, *Chem. Eur. J.* **2009**, *15*, 5926.
[114] M. D. Tissandier, K. A. Cowen, W. Y. Feng, E. Gundlach, M. H. Cohen, A. D. Earhart, J. V. Coe, T. R. Tuttle, *J. Phys. Chem. A* **1998**, *102*, 7787.
[115] C. P. Kelly, C. J. Cramer, D. G. Truhlar, *J. Phys. Chem. A* **2006**, *110*, 16066.
[116] C.-G. Zhan, D. A. Dixon, *J. Phys. Chem. A* **2001**, *105*, 11534.
[117] W. R. Fawcett, *Langmuir* **2008**, *24*, 9868.
[118] S. Trasatti, *Pure Appl. Chem.* **1986**, *58*, 955.
[119] R. G. Pearson, *J. Am. Chem. Soc.* **1986**, *108*, 6109.
[120] A. V. Marenich, J. Ho, M. L. Coote, C. J. Cramer, D. G. Truhlar, *Phys. Chem. Chem. Phys.* **2014**, *16*, 15068.
[121] D. M. Chipman, *Theor. Chem. Acc.* **2002**, *107*, 80.
[122] J. P. Perdew, K. Schmidt, *AIP Conf. Proc.* **2001**, 577, 1.
[123] J. F. Janak, *Phys. Rev. B* **1978**, *18*, 7165.
[124] E. Baerends, O. Gritsenko, R. Van Meer, *Phys. Chem. Chem. Phys.* **2013**, *15*, 16408.
[125] V. Atalla, I. Y. Zhang, O. T. Hofmann, X. Ren, P. Rinke, M. Scheffler, *Phys. Rev. B* **2016**, *94*, 35140.
[126] L. Goerigk, A. Hansen, C. Bauer, S. Ehrlich, A. Najibi, S. Grimme, *Phys. Chem. Chem. Phys.* **2017**, *19*, 32184.

SUPPORTING INFORMATION

Additional supporting information can be found online in the Supporting Information section at the end of this article.

How to cite this article: A. J. Achazi, X. Fataj, P. Rohland, M. D. Hager, U. S. Schubert, D. Mollenhauer, *J. Comput. Chem.* **2024**, *45*(14), 1112. https://doi.org/10.1002/jcc.27299